Spatial and temporal variation of vertical profiles of rainfall rate observed by spaceborne precipitation radar
(衛星搭載降雨レーダで観測された降雨強度鉛直プロファイルの時空間変動に関する研究)

Masafumi Hirose

Division of Earth and Planetary Science,
Graduate School of Science,
Nagoya University

(広瀬 正史 名古屋大学 大学院
理学研究科 地球惑星理学専攻)

January, 2004

報告番号	甲第 6189 号

ABSTRACT

The Tropical Rainfall Measuring Mission/Precipitation Radar (TRMM PR) has made it possible for the first time to evaluate global characteristics of vertical structures of rainfall. This study is intended to depict features of seasonal and spatial variations of the vertical gradient of rainfall rate using TRMM PR data from 1998 to 2000.

The features of Downward Decreasing (DD) or Downward Increasing (DI) rainfall rate in the lower part of the vertical profile are focused on. Horizontal maps were made showing decreasing/increasing characteristics in the vertical gradient of rainfall rate over monsoon Asia. The pattern showed a clear land-ocean contrast and had monthly variation as the monsoon progressed in Asia. The DD pattern migrated northward around the monsoon onset and withdrew southward in the retrogressing period. The seasonal march of the DD pattern was clear especially over the India subcontinent. The DD seemed to be bordering monsoon rainfall over India. The general and local characteristics were further examined over the global tropics. DD profiles dominated tropical interior landmasses such as Africa and the Brazilian Plateau in summer. DI profiles were observed over land in winter and over ocean except for regions with very little rainfall. In addition, DI profiles appeared during the height of the wet season even over the tropical landmasses, such as the mature monsoon period over inland India and over the Amazon River basin.

Individual precipitation systems were also investigated in terms of their areally averaged DD and DI characteristics mainly over India. Deep (shallow) profiles tended to be DD (DI) for all seasons except the premonsoon season. As the rain area increased, the vertical gradient of rainfall rate decreased (DD tendency). Embedded in the dominant DD signature for deep storms, deep but significant DI profiles were observed in every month. They characterized the precipitation in the premonsoon season. More than half of the mesoscale/synoptic-scale systems (rain areas$>10^4$ km^2) having the significant DD or DI regions had both of them as part of their slant cores. The vertical gradients for these systems had a similar trend for both their stratiform and convective parts. During the mature period of the southwest monsoon, the number of small systems that were DI and widespread systems with moderate vertical gradient increased.

A series of results showed that the relationship between the scale and the internal structure of precipitation systems have seasonal and spatial variation. The different composition of precipitation systems inferred that the convective activity over dry season is closely associated with atmospheric circulation. Abundant water vapor would change the internal structure even they are similar-scale systems.

Contents

1. Introduction

1.1 Background

The study and continuous measurement of precipitation systems is indispensable for understanding the climate system and the global water cycle. Distinguishing the local variation from the general characteristics of precipitation systems would be a good step to understanding the dynamical and thermodynamical mechanisms of the systems and microphysical processes therein (*e.g.,* Houze 1981; Zipser and Lutz 1994). These "precipitation regimes" include the easterly and westerly flow regimes in the Amazon area, onset and mature phases of the monsoon, and well-known El Niño and La Niña episodes (*e.g.,* Petersen and Rutledge 2001; Rickenbach *et al.* 2002).

The Asian summer monsoon is known for abundant rainfall that has spatial and seasonal variations (Webster *et al.* 1998). A large number of studies have been made on the monsoon rainfall. It has been shown that changes in surface albedo, surface roughness, soil moisture, evapotranspiration, and vegetation, etc., affect local rainfall (see Chang and Krishnamurti (1987), Chapter 2 and references therein). For example, Webster (1983) examined ground hydrological effects related to processes in large-scale atmospheric dynamics using a numerical model. He depicted mechanisms of monsoon low-frequency variability, in which the evaporative cooling of the moist ground reduces the sensible heat input to the atmosphere and effectively stabilizes the troposphere and, hence, reduces the convective heating. He concluded that ground hydrological effects may explain the seasonal variability of rain. Thus, it is considered that differences of physical processes, which rain changes, could affect the vertical structure and evolution of precipitation systems. A survey on vertical profiles of monsoon rainfall carries this understanding one step further.

The large seasonally varying differences of precipitation systems include that of the vertical structure (*e.g.,* Berg *et al.* 2002). There has been an increase in the num-

ber of studies on the characteristics of three-dimensional rain structure, which include the classification of convective and stratiform rain, not only for the precipitation climatology, but also for the successful retrievals of surface rainfall and latent heating profiles (Lang *et al.* 2003; Tao *et al.* 1993; Shige *et al.* 2003). For example, the convective-stratiform partitioning methods are expected to provide a comprehensive view of the rain type by understanding hydrometeors and atmospheric motion at each levels (Lang *et al.* 2003). The observational data, by developed technology and retrievals, offer a major step forward in documenting and understanding one for above-mentioned potential demand in the precipitation climatology.

1.1.1 Global precipitation measurement

The effort to depict a global map of precipitation is ongoing, requiring huge amounts of homogeneous data over the globe (*e.g.,* Xie and Arkin 1996). In situ or satellite data are assimilated and are used to generate gridded rain maps that are intercompared (Gates *et al.* 1999; Gruber *et al.* 2000; Sorooshian *et al.* 2000). To accurately observe spatial and temporal fluctuations of rain in the Tropics is still an important and difficult task. Ground-based observation by a radar network is generally very limited and localized, and it is impossible to observe the vertical structure of rain on a continental or global scale. Observation from space is suitable to generate a global and homogeneous dataset for a long period of time, and it is essential for providing the global distribution of rain. The accuracy is, however, still insufficient. There have been technical difficulties in the retrieval of the three-dimensional precipitation structure from satellite measurements. The infrared-based rainfall estimate itself still has difficulties such as in the discrimination of nonprecipitating clouds, so many recent strategies are focused on merging rainfall estimates from several sources such as microwave data (*e.g.,* Xu *et al.* 1999). The use of observations with microwave imagers has been restricted to oceans due to the difficulty of discriminating the emission of raindrops from that of land. The retrieval technique has developed further with recent improved algorithms (Kummerow *et al.* 2000). Even with limitations, these large-scaled observations are successfully used to make horizontal rain maps. However,

observation of the vertical rain structure on a global scale is much more difficult. Even though huge amounts of data are accumulated by passive techniques, they are insufficient to describe the spatial diversity of rainfall because of the poor capability of profiling.

Thus, the Tropical Rainfall Measuring Mission (TRMM) equipped with the first spaceborne Precipitation Radar (PR) was launched in 1997. It has provided a nearly homogeneous dataset of rainfall rate suited for rain-type estimation and the structure in the horizontal and vertical directions over land and ocean (Awaka *et al.* 1997; Iguchi *et al.* 2000). Data obtained with the active sensor were long awaited (Simpson *et al.* 1988). It has made possible the statistical depiction of seasonal variations of global rain, but it cannot observe the dynamic evolution of individual storms. We are now able to evaluate various profiles of rain with instantaneous and statistical data. This progress gives us a chance to study the statistics of vertical profiles of rain.

1.1.2 Statistical researches of vertical rain profiles

Several kinds of precipitation climatology have been reported using the TRMM PR data. Liu and Fu (2001) and Fu and Liu (2001) investigated the principal modes and variability of rainfall-rate profiles especially around the Tropics using TRMM PR data and explained physical processes inferred from the profiles. They showed that profiles with significant rain appeared in the mature period and characterized mean profiles. Their results showed that the slopes of the profiles divided vertically into three or four layers were approximately constants on a logarithm scale. They implied that there is a common physical process working in the tropical cloud systems that determines the general pattern of the vertical profiles of rain. They also observed the seasonal variation of vertical profiles around midlatitudes. Maxima of profiles were explained as changes of brightband height in stratiform rain and the height of intensive rain in convective rain. A decrease in reflectivity in the lowest part of the profile was considered to imply that raindrops experience no further growth or may undergo slight evaporation. Takayabu (2002) prescribed individual rain profiles in spectral representation. These approaches of dealing large set of vertical rainfall-rate structure data allowed us to understand what the statistics or instantaneous

snapshots indicate. Composite analyses between vertical and horizontal pattern would be a key to understand the impacts of individual systems to precipitation climatology (*e.g.,* Stano *et al.* 2002). For classifying the precipitation systems, storm height, rainfall rate at near surface, and bright-band existence have been mainly used as rain-type indices. Precipitation-system structure is dictated by parameters of stratiform rain fraction, bright-band height, and rainfall at the bright band, in addition to the above-mentioned factors (Shige *et al.* 2003; Schumacher and Houze 2003a; Tao *et al.* 1993).

Physical processes have regional or seasonal variation. If we know the behavior of rainfall with large spatiotemporal extent, we would be a step closer to understanding the phenomena of seasonal variation of rain, which may be an indicator of the operating physical processes.

1.1.3 Implications of vertical distribution of rainfall rate

Much can be said on the implications of vertical distribution of rainfall rate. A downward increase in mass flux indicates precipitating hydrometeors growth due to coalescence (*e.g.,* Liu and Fu 2001). Convection with low core height could be another possible reason for downward increasing rainfall rates. On the other hand, one interpretation for a downward decrease in water flux is evaporation (*e.g.,* Fu *et al.* 2003; Adeyewa and Nakamura 2003). In several models, the rate of change of rainwater mixing ratio ($\overline{q_r}$) due to evaporation of raindrops is derived from the magnitude of rainwater mixing ratio, temperature, pressure, sub-saturation, and Reynold's number (*e.g.,* Syono and Takeda 1962; Tripoli and Cotton 1980). Katzfey and Ryan (1997) reported that evaporation in the unsaturated sub-cloud layer near the surface reduced the rainfall percentage significantly for stratiform rain. Rosenfeld and Mintz (1988) investigated the downward decrease in rainfall under cloud-base, around 1–2.2 km, for rainshafts in summer convective cells in a semi-arid region. The effects of evaporation strongly depend on precipitation type which is associated with the vertical velocity, rainfall intensity (Takemi 1999), and the surrounding environment. There are other possible factors with regard to a downward decreasing rainfall rate. Hydrometeors suspended aloft can be influenced by strong updrafts and lateral transport

by the horizontal flow. Suspended hydrometeors in the initial stages of precipitation can generate a slight maximum rainfall rate aloft even though it is generally weak. Differences in raindrop fall velocities in strong updrafts and downdrafts or differences in hydrometeors (e.g., graupels) can influence rainfall-rate retrieval through Z–R relationships (*e.g.,* Atlas *et al.* 1973; Battan 1976; Dotzek and Beheng 2001; Dotzek and Fehr 2003; Matejka *et al.* 1980; Rutledge and Hobbs 1984; Salles and Creutin 2003).

Mesoscale Convective Systems (MCSs) or storms with significant vertical shear show clear vertical tilt or a non-downward flux of hydrometeors (*e.g.,* Klemp and Wilhelmson 1978; McAnelly *et al.* 1997; Parker and Johnson 2000; Rutledge and Houze 1987). The combined effect of lateral and upward flux on water loading means negative buoyancy may be non-negligible for average vertical profiles. Precipitation events often occur in complex combinations of stratiform and convective patterns. Some insight could be gained by examining a large data volume showing the dynamic variation of precipitation-system structure.

Further possible explanations can be obtained then from observations of individual precipitation systems with various scales in time and space. The global climatology of the vertical gradient of rainfall rate can characterize precipitation-system structure more concretely.

1.2 Objectives and outline of this thesis

These a few years have seen a renewal of interest in the time-space variation of precipitation by the TRMM PR. However, it has not been studied deeply about the seasonal and regional variation in the vertical structure of precipitation systems over various climatic regions, although it is one of the hot topics for the discussion to establish some standards for precipitation climatology. The purpose of this study is to clarify the characteristics of vertical profiles of rainfall rate and the differences in season and region, and to discuss with the general and local features of precipitation systems.

Precipitation datasets and method of analyses are described in Chapter 2. Chapter

3 deals with the vertical rain profiles in Asian summer monsoon and represents the seasonal variation. Section 3.1 presents the general features of near-surface rain over Asia. In Section 3.2, the regional features of the vertical profile of rainfall rate are described, and a new index on the vertical gradient of rainfall rate is introduced in Section 3.3. Section 3.4 documents the characteristics of the vertical rain profiles in terms of the index. Section 3.5 presents the results on the seasonal variation mainly over the Indian subcontinent. In Section 3.6, statistical relationships between the vertical gradient and the horizontal extent are examined. Chapter 4 describes the seasonal and regional differences of the vertical gradient of monthly rainfall rate and qualitative analyses of individual rainfall-rate profiles and individual precipitation systems over various climatic regions such as tropical interior landmasses and highly-wet regions. In Section 4.1, a global map of the index and the characteristics are depicted. Section 4.2 presents several parameters for individual rain profiles. Section 4.3 explores the population of individual systems over distinct geographical regions. The findings are summarized and discussed in Chapter 5. A general conclusion of this study is summarized in Chapter 6.

2. Data and method

2.1 TRMM

The TRMM satellite orbits between 35°S–35°N in a non-sun-synchronous orbit. It is equipped with the PR, the TRMM Microwave Imager (TMI), the Visible Infrared Scanner (VIRS), the Clouds and Earth's Radiant Energy System (CERES) and the Lightning Imaging Sensor (LIS). One of the main purposes of this mission is to measure the total amount of rain for each month over 5° × 5° latitude-longitude grid cells. An improvement in the estimation of rainfall rate and latent heat release profiles over the globe is expected.

The data fall into four levels. Level 0 is for raw data. Level 1 is for engineering data, and level 2 is for estimated physical data. Then, Level 3 is for monthly statistical data.

In this study, 3 yr of data during 1998–2000 were used to extract a climatological feature over the Asian region (10°S–40°N and 60°–150°E) and over the globe between 35°S–35°N. We mainly used the TRMM PR product designated 2A25 to investigate the rain structure in detail. In chapter 3, the 2A23 product and the 3A25 product were also used to map storm height histograms and to obtain monthly rain statistics, respectively. Version 5 of the TRMM PR algorithms was used.

2.2 PR data

The most unique characteristic of the TRMM PR is its capability to observe the three dimensional structure of rain from space. The output of rainfall rate is produced considering drop size distributions implicitly as stated below. It may be safely assumed that it is most reliable three-dimensional dataset of rainfall rate at present. We use the rainfall rate instead of observed reflectivity (Z). Vertical resolution is 250 m, while horizontal

resolution is 4.3 km at nadir.

Product 2A23 provides rain types, and the storm height, which is the top altitude of the three highest consecutive range bins with significant echoes (> 17 dBZ). The heights of clouds or convection differ from those of precipitation. We consider the precipitation top height as the "storm height" in this study. In this paper, the altitude is from Earth's ellipsoid instead of from the surface. The algorithm classified precipitation type into three categories: stratiform, convective and others, considering the vertical and horizontal distribution of reflectivity (Awaka *et al.* 1997). The V-method, which stands for vertical method, uses the existence of a bright band, and the height and intensity of maximum reflectivity. The H-method, which stands for horizontal method, is basically on a method proposed by Steiner *et al.* (1995). This method uses the horizontal rain distribution of the strongest echo for each profile.

Product 2A25 is the principal instantaneous TRMM PR dataset detailing the rain structure (Iguchi *et al.* 2000). The main data included are the attenuation-corrected radar reflectivity factor (Z) and the rainfall rate (R). The rainfall rate is estimated from each corrected Z factor using suitable Z–R relationships. The algorithm uses empirical coefficients for Z–R relationships at five levels for each profile. The five levels depend on rain types, height of bright band (if it exists), 0°C level estimate, and altitudes of storm height. The coefficient depends on rain types, the assumed particle phase at each level, and terminal velocity. In addition to those, a beam filling effect correction is also applied. The coefficients between the levels are interpolated linearly.

A considerable amount of validation has been performed to certify that the estimated near-surface rainfall rate is reliable (*e.g.,* Kummerow *et al.* 2000; Bolen and Chandrasekar 2000; Schumacher and Houze 2000). Here, "near surface" means the lowest level free from ground clutter, which is around 500 m above the surface at nadir. However, some problems still remain in validating the three-dimensional structure of precipitation. One such problem is associated with the bright band. Conventional knowledge is not yet good enough to physically validate of rainfall rates around the bright band derived from current algorithms. Rainfall profiles show spikes around the bright band and have less

accuracy. The second problem is the technical difficulty in producing fully homogeneous three-dimensional datasets. Detection of the bright band needs high vertical resolution. However, at the edge of the PR swath, height smearing is intolerable, being more than 1 km. Data near the scan edge contains factors that deteriorate the vertical profiles such as height smearing, a slanting incident mainlobe, and masked regions at low levels from sidelobes in the nadir.

To mitigate the aforementioned factors, the rainfall rate around the bright band was replaced with linearly interpolated data using data $\pm$750 m from the bright band peak. And secondly, only data with a swath angle within 7° from nadir was used. The number of the available field of views (FOVs) in the cross track was 21 out of a total of 49. The analyzed width being around 86 km out of the available 215 km width of the TRMM PR for each cross track scan. Awaka (1998) reported that 80 % of bright bands are detected correctly within 7° of nadir.

The above-mentioned procedure was used through out the study except in estimating rain area. Rain flag data was used in all angle bins to estimate the size of a precipitation system more accurately. The rain flag is defined when significant rain signal exists in the FOV. The minimum detectable radar reflectivity of the PR is 18 dBZ ($\sim$ 0.5 mm h^{-1}) where the signal-to-noise (S/N) ratio is nearly 0 dB at storm top. Values around 13 dBZ corresponding to weak rainfall rates are also observable though it depends on the system noise level.

The area of each precipitation system and the fraction of convective area (individual as well as total) were calculated as follows. First, a flag is checked on a pixel where rain is certain to exist. Next, nearby rain pixels are used to identify a common precipitation system using neighboring flags within about ten kilometers. The neighbors within the ten kilometers are recognized as being part of the same system as are the pixels adjacent to them. Contiguous systems are determined through iteration. The "rain area" is calculated approximately by multiplying the number of connecting pixels by 15 km^2 as the footprint size is about 4.3 km at nadir and increases only by 0.8 % 7° off nadir. Areas of individual convective rain are derived from a similar procedure using a "convective" flag instead of

a rain flag. The total convective rain area is defined as the summation of all embedded convective pixels in the same precipitation system. The area of large systems will, however, be underestimated due to the TRMM PR swath (Nesbitt *et al.* 2000).

We made $5° \times 5°$ and $1° \times 1°$ datasets. Each $1° \times 1°$ box of our 2A25 database using narrow swath has a sampling number of more than 2000 fields of view. For example, each grid over tropics or subtropics contains at least several hundreds of fields of view for each quarter of a day, while the sampling number for a certain local time in each month is not uniform even using three years of data. Thus the data sampling, which includes some aspects of diurnal cycles, is adequate to carry out a study of seasonal variation. We used data above 2 km from ellipsoid in our statistical analyses considering the following surface detection algorithm. Only echoes that are sufficiently discriminated from the surface are recognized as rain, and otherwise the range bin data are flagged as surface-contaminated. Thus, strong rain is picked up in the near-surface range bins, which does not affect significantly the rainfall amount statistics or instantaneous data but causes biased rainfall rate statistics (mostly below 1.5 km).

We also used product 3A25 which is suitable for the analysis of seasonal rain variations. The monthly statistics of rain were calculated over fine grids of $0.5° \times 0.5°$ latitude/longitude resolution and coarse grids of $5° \times 5°$. The outputs include monthly averaged rainfall rate at six layers (near surface, 2, 4, 6, 10 and 15 km) and the path average rainfall rate for coarse grids, and at four layers (near surface, 2 km, 4 km and 6 km) and path average rainfall rate for fine grids. We used 3A25 data to capture the horizontal and seasonal characteristics of rain distribution. We averaged near surface rainfall amount, rainfall rate, storm height and fraction of each rain type over Asia during 3 yr from 1998 to 2000.

2.3 Other data

We used the Global 30 Arc Second Elevation Data Set (GTOPO30) produced by the Earth Resources Observation Systems (EROS) Data Center of U.S. Geological Survey

to obtain the topographical map. The resolution is 1 km in the horizontal and 1 m in the vertical. In this research, data averaged over $0.5^\circ \times 0.5^\circ$ are used.

In order to check the wind field as in Fig. 1, we used the National Centers for Environmental Prediction-National Center for Atmospheric Research (NCEP-NCAR) reanalysis data (Kalnay *et al.* 1996; Trenberth and Guillemot 1998). The arrows in the figure show horizontal wind fields at 850 hPa and 200 hPa averaged from May to October during 1998-2000. The data of precipitable water in Section 4.1 were also derived from the NCEP-NCAR reanalysis data.

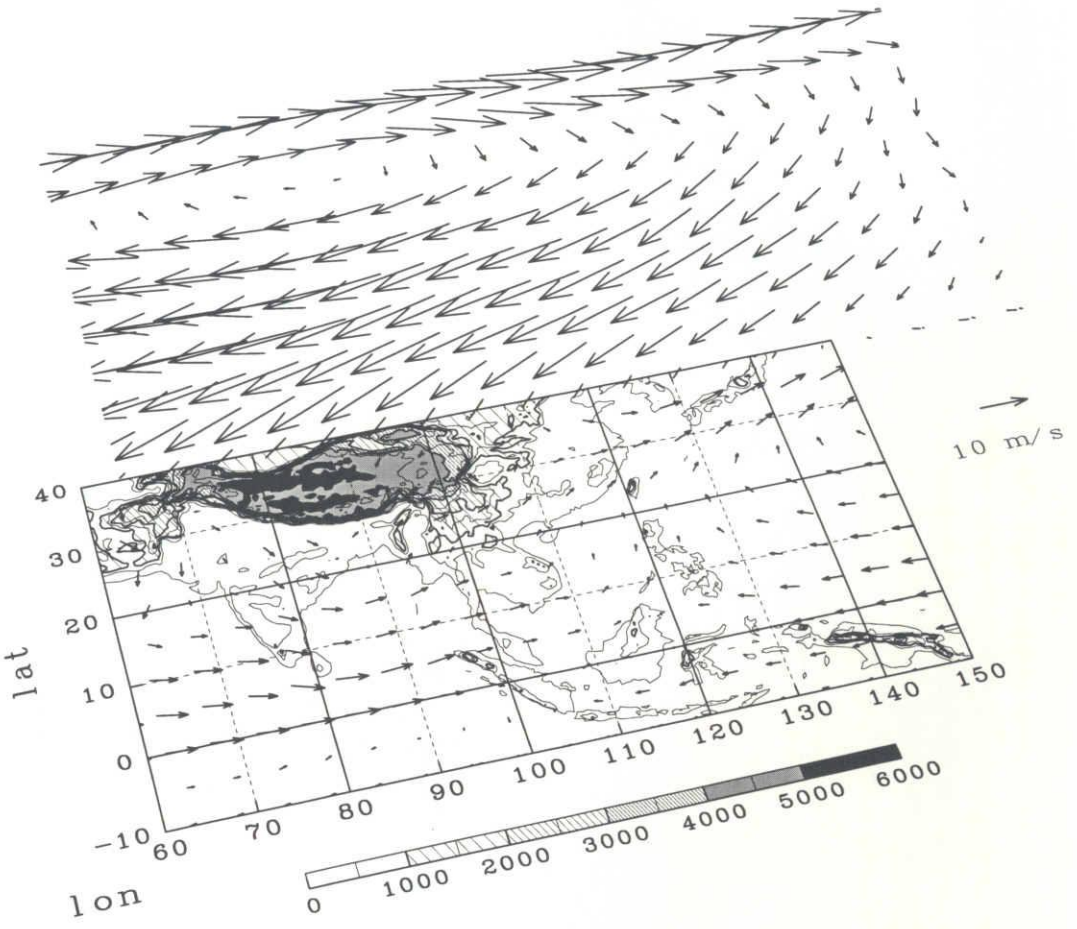

Figure 1. Wind field for analyzed area along with topographical map. The contours are drawn with a 500 m height interval. The upper (lower) arrows show the wind averaged for three summer seasons (from May to October during 1998–2000) at the 200 (850) hPa level.

3. Spatial and seasonal variation of rain profiles over monsoon Asia

3.1 General features of near surface rain

To begin, we will examine distributions of near surface rain. Figure 2 shows horizontal rainfall distributions for the monsoon season from May to October over Asia using 3A25 data. In the monsoon season, there is much precipitation over not only the equatorial zone but also the coastal ocean and land such as the western coast of Indochina (Fig. 2a). We focus on the Asian rain to see the distribution in detail. Figure 2b shows averaged near-surface rainfall over 10°S–40°N, 60°–150°E. Figure 2c shows the distribution of the conditional rainfall rate, that is, the rainfall rate conditioned on rain.

Figure 2b shows clear topographic effects on the rain distribution. The figure shows concentrations of rain on the southwestern side of mountains or coasts where low-level humid wind blows in from southwestern oceans as indicated in Fig. 1. The rain expands from the coastline westward over oceans, such as the Indian Western Ghats, the Arakan Mountains, the Bilauktaung Range in Myanmar and Barisan Mountains on the island of Sumatra. Other rainy regions are at the southern foothills of the Himalayas, the western sides of the islands of Luzon, Kalimantan, New Guinea, and Japan. As a whole, the rainfall amount seems to be larger over the ocean than over land, especially around coastal regions. We recognized similar characteristics for 6-month averages in each year from 1998 to 2000, although there were variations in the timing and quantity of rainfall such as more rainfall amount over the southwestern ocean of Sumatra in 1998 (not shown).

The strong conditional rainfall-rate regions in Fig. 2c are noticeable over north of the Thar Desert (Punjab), the South China Sea, the Java Sea, the island of Java, East of India, the Strait of Malacca, and southwest of Japan. The pattern of conditional rainfall rate does not relate to rainfall amount. Weak (strong) precipitation falls a lot (a little) over the western coast (the eastern coast) of India and Indochina.

The characteristics of conditional rainfall-rate profiles corresponding to these general features over this region of Asia are addressed in the following section.

3.2 Regional features of the vertical profile

We made a 5° × 5° dataset over Asia for 10°S–40°N, 60°–150°E from May to August; namely, from the onset to the mature period of the Asian monsoon, from our 2A25 subsets. We examined vertical profiles of conditional rainfall rate and storm height histograms for stratiform and convective types for each grid cell. As mentioned before, conditional rainfall rates in the brightband layer are interpolated using data above and below the bright band.

Figure 3 shows typical examples of the vertical profile of conditional rainfall rate and storm height histograms over land (region A: 15°–20°N, 75°–80°E for India) and ocean (region B: 15°–20°N, 135°–140°E in the western Pacific) in May. These regions do not have significant orographic effects such as coastal mountain ranges shown in the rainfall map (Fig. 2b). The storm height histogram shows that precipitation over land has only one gentle peak around 6 km (5 km for stratiform and 7 km for convective rain) and no peak in lower levels. Such unimodal structure characterizes rain over the continents or the continental-like regimes (Petersen and Rutledge 2001). Over ocean, shallow and marginally high storm peaks appear. This is a common feature as reported by Short and Nakamura (2000). The conditional rainfall rate profile over land has a peak around 3–3.5 km just below the storm height histogram peak. On the other hand, the conditional rainfall rate profile over the ocean has no maximum and monotonically decreases with height. Though the histograms of storm height show peaks at the bright band, conditional rainfall rate profiles have no maximum there due to our linear interpolation.

Maximum hydrometeor contents aloft have been commonly seen in snapshots of radar observations and in model representations (*e.g.,* Rutledge and Hobbs 1984; Rutledge and Houze 1987; Westcott and Kennedy 1989; Williams *et al.* 1989). However, the interpretation of these peaks shown in profiles averaged over large regions has remained

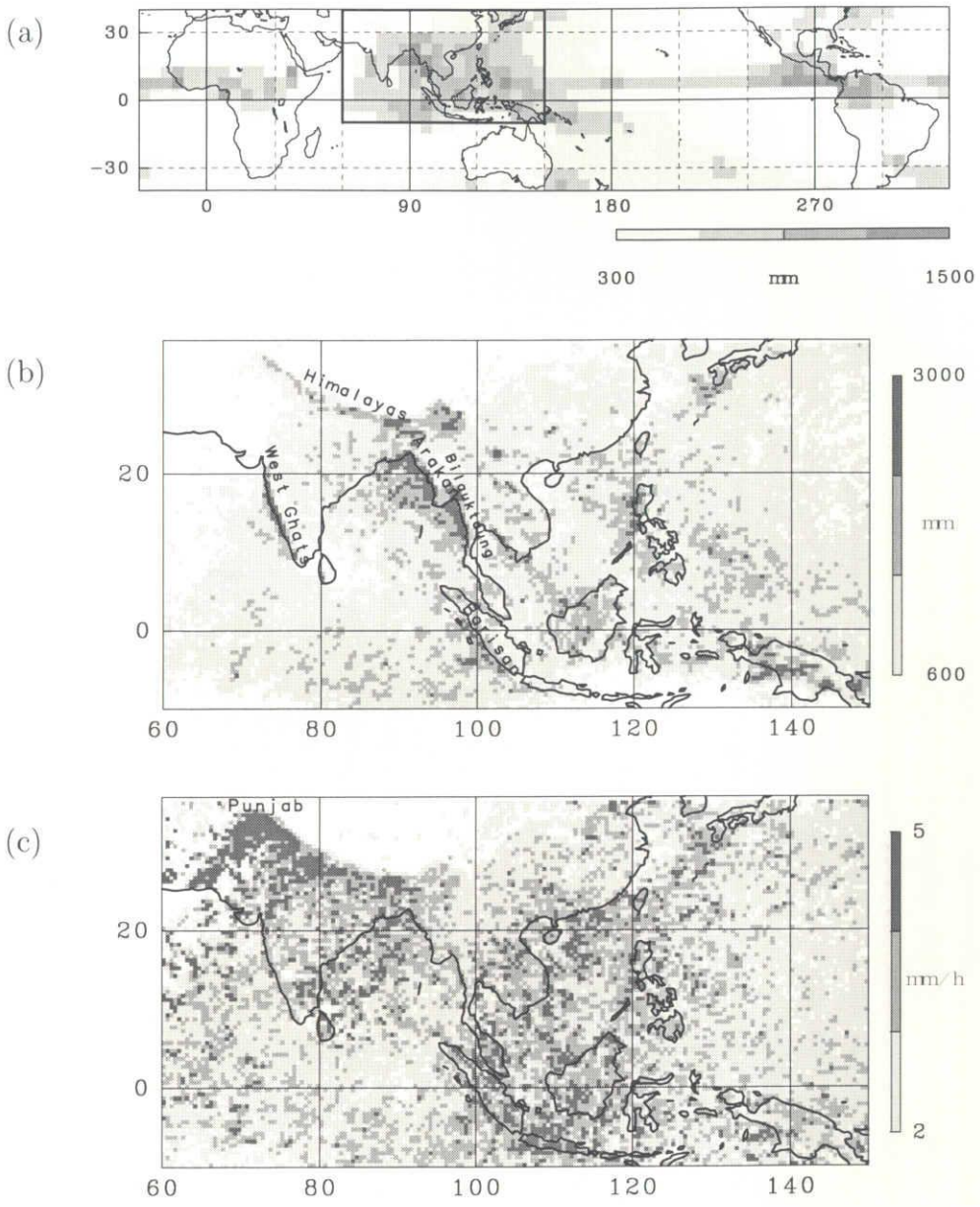

Figure 2. Distribution of the near surface rain averaged for the summer seasons. (a) World map of rainfall amount. (b) Rainfall amount over Asia in mm with name of mountain ranges. (c) Conditional rainfall rate in mm h^{-1}.

uncertain since statistical analyses of the vertical rainfall-rate profiles over large areas have been difficult. Large-scale and seasonal mapping of this type of index was impossible before the TRMM PR.

Rain activity depends strongly on the season and location. The above-mentioned characteristics seem to be general but there are many exceptions. For example, rain over Bangladesh is much different from that over region A. If we compare conditional rainfall-rate profiles over land and over ocean for the whole analyzed area, we do not see such clear differences. Hereafter we will examine how such characteristics distribute horizontally.

Also, caution must be taken in interpreting the downward decrease in rainfall rate below the maximum as attenuation is significant and present in TRMM PR data (*e.g.*, Liu and Fu 2001). However, the attenuation correction for reflectivity profiles was validated by a ground-based radar (*e.g.*, Bolen and Chandrasekar 2000) and is assumed to be well corrected in this study.

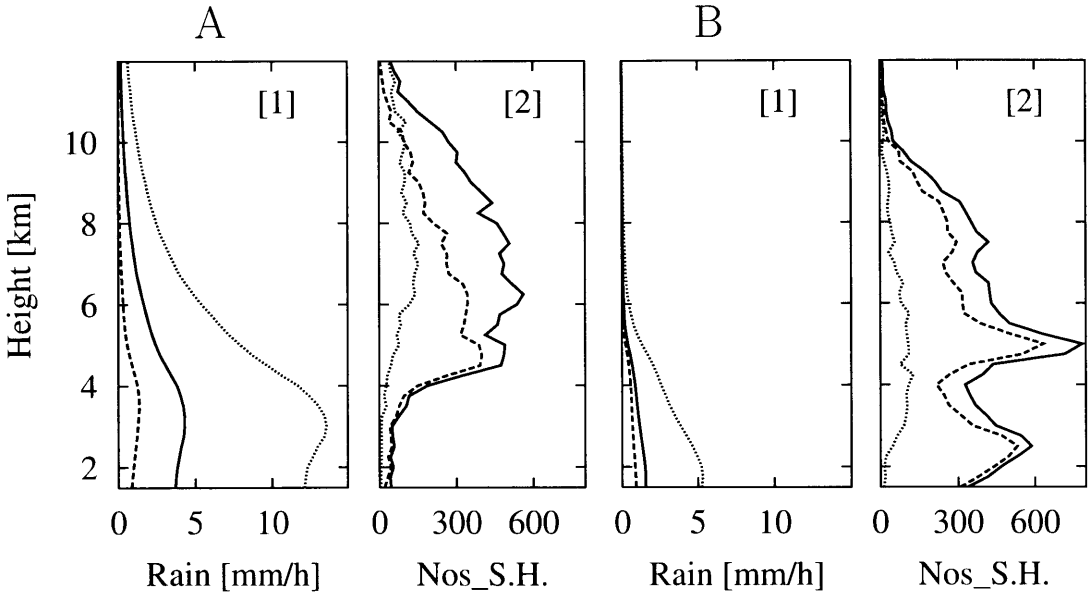

Figure 3. Conditional rainfall rate profile [1] and storm height histogram [2] over region A (15°N–20°N, 75°E–80°E) and B (15°N–20°N, 135°E–140°E) in May, respectively. Lines show all rain (solid), stratiform (dashed) and convective rain (dotted).

3.3 Index of vertical gradient

3.3.1 Downward decreasing or increasing rainfall rates

The vertical profiles of the conditional rainfall rate may be divided into two types: downward decreasing and downward increasing. The downward decreasing or a modal structure has been described for the Z profile (*e.g.,* Liu and Fu 2001; Fu and Liu 2001). As Houze (1981) illustrated for convective rain, growing precipitation particles can be suspended or carried aloft by strong updrafts. An example of the radar-echo life cycle of a single-cell thunderstorm was shown in a figure of time-height evolution of maximum radar reflectivity (Williams *et al.* 1989). In their studies, the gradient of Z is not directly related to physical quantities such as the water flux due to the variety of drop size distributions and is simply interpreted as the possibility of raindrop evaporation. Considering that attenuation of reflectivity is well corrected (*e.g.,* Bolen and Chandrasekar 2000), one explanation for the characteristics may also be that the downward decreasing profile corresponds to evaporation in the lower atmosphere or duration of suspension of raindrops due to updrafts, and the downward increasing corresponds to shallow precipitation or systematic events with low level convergence. We made vertical differential profiles by taking the difference of conditional rainfall rates at consecutive range bins. Negative (positive) values indicate a downward decreasing (increasing) rainfall rate.

The vertical differential profiles are shown in Fig. 4, in which downward decreasing and increasing are shown by negative (contours) and positive (gray shadings) values. The grid data at $5^\circ \times 5^\circ$ resolution and the contour generating routine made the distribution smooth. The abscissa indicates the longitude. The figure shows the pattern for all, stratiform and convective rain types, respectively, from the top along with a map of the data region shown in the bottom image. Regarding the profile, contoured regions, that is, downward decreasing regions, appear over land. We have a distinct dark region, that is, downward increasing, around 5 km. We also notice another dark layer at about 3 km over ocean in the convective case. It also exists in other images but not clearly seen. In Fig. 4 (middle, stratiform rain), the values are nearly zero except for a narrow layer around 5

km and for the downward decreasing over India. This shows that the average profile of stratiform rain is more likely a "shelf" type. In Fig. 4 (bottom, convective rain), the dark layer expands both upward and downward compared to the stratiform case.

Figure 5 shows vertical differential profiles over Asia in May within each 5°×5° latitude-longitude box. Every 5° in latitude correspond to the altitude from 2 to 5 km. For example, 2-km altitude corresponds to 10°N and 5 km to 15°N in the case of the vertical difference of the conditional rainfall rate over 10°–15°N. Since the height is from the ellipsoid, which is approximately mean sea level, we have no data available over high land regions. We exclude data if the number of rain pixels is less than 100. We also exclude data points for which the number of pixels in the 5°×5° box is within 90 % of the total sampling number due to geographical variations, for example, over the Tibetan Plateau. The figure tells us clearly that the downward decreasing (contours) appear over land particularly over India in this season.

We made an index that shows the decreasing–increasing characteristics. The index is the difference of conditional rainfall rates at 2 and 3.5 km divided by 1.5 km. The unit is mm h^{-1} km^{-1}. The lower altitude of 2 km was determined by considering the sampling numbers. The sampling number decreases significantly below 2 km height over land. In addition, we want to avoid the low level statistical problem associated with the surface detection algorithm mentioned in Section 2.2. The upper altitude of 3.5 km was determined to be around the level of significant echo peaks and to avoid the trace of the bright band. Hereafter, we will call it the "index of vertical gradient" (IVG) and use the terms "downward decreasing" (DD) and "downward increasing" (DI) to refer to a decrease or increase of the conditional rainfall rate at the low level.

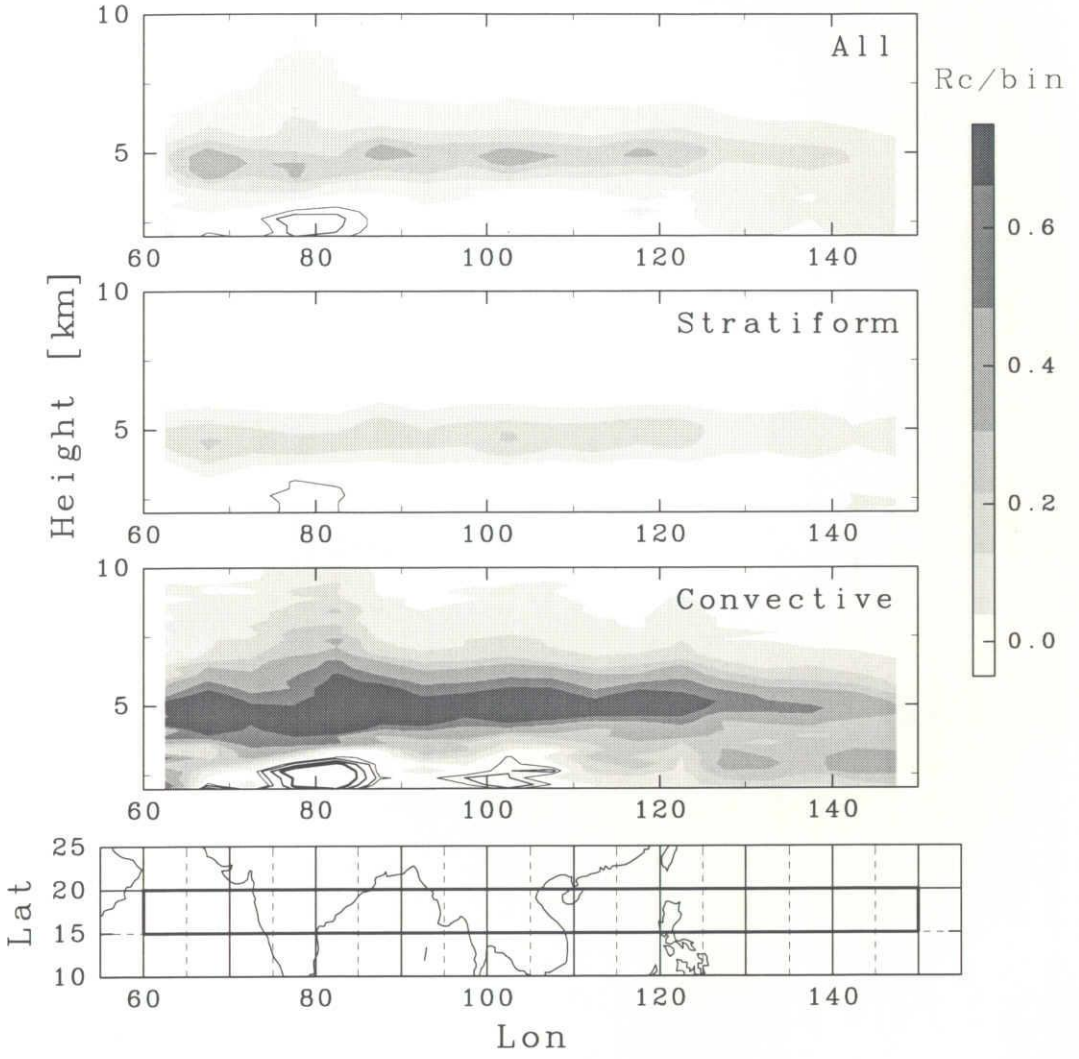

Figure 4. Vertical difference of conditional rainfall rate for each range bin. The conditional rainfall rate is averaged for 5 × 5 degree boxes over 10°N– 15°N, 60°E–150°E in May. The unit is mm h^{-1} 250m^{-1}. Contours are at -0.05, -0.1, -0.2, and -0.3 mm h^{-1} 250m^{-1}.

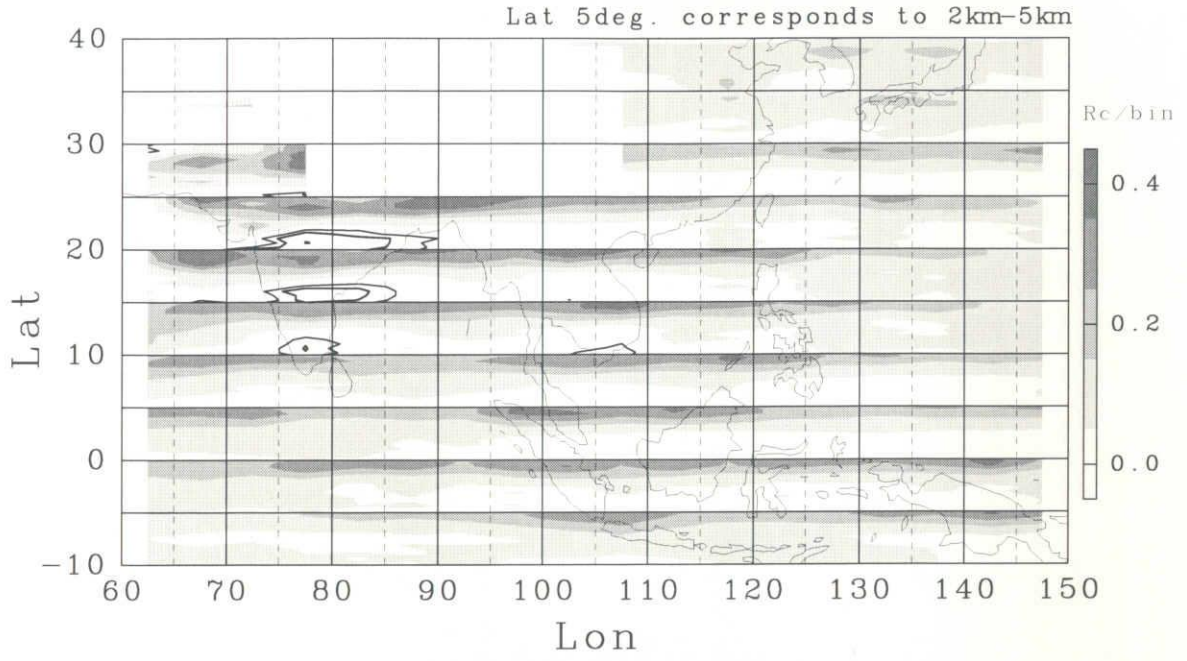

Figure 5. Horizontal map of vertical difference for all rain in May. Each increment of 5° in latitude corresponds to the height from 2 km to 5 km. Region with high mountains or without rainfall are excluded. Contours are at -0.05, -0.1, and -0.2 mm h^{-1} $250m^{-1}$.

3.3.2 Profiles indicated by IVG

Investigation of the large number of vertical profiles revealed that DD contained most of the significant modal structures of rainfall rate. Figure 6 shows monthly accumulated rainfall-rate peak and storm-height histograms over inland India (5°–25°N, 65°–90°E). In studying the IVG over different regions, "inland" is selected in such a way that the orographic effects are minimal. The "coastal (inland)" region is defined as having land within (not within) 1° of an oceanic grid. In the coastal upwelling region, mountains such as the Western Ghats obstruct the large moist inflow and generate copioous orographic DI rain as shown in later section. A rainfall-rate peak was simply defined as a center point between three consecutive range bins (±750 m) of positive and negative vertical gradient of rainfall rate. Rainfall-rate peaks are concentrated around 4 km for stratiform rain (Fig. 6a). However, the peak at 4 km in the stratiform histogram does not indicate a rainfall rate maximum . The peak generally appears at 750 m below the bright band peak since it tends to be an inflection point induced by the interpolated data after removing the original data near the bright band. The concentration of rainfall rate peaks at 4 km shows that the 3.5 km level is not affected by the profile modification for the bright band.

The histogram for convective rain (Fig. 6b) shows large variations with height but with a constant peak magnitude. The peaks in frequency varied several hundred meters in phase with the storm heights; however, the peaks disappeared in winter (not shown in Fig. 6b). It seems reasonable to use a constant level of 3.5 km as it is around or beneath the central level of peaks. This study did not consider the low-level peaks that appeared around 2 km, associated with shallow convection, since robust statistics are needed with sufficient samples for the most significant peaks. The fact that IVG in general does not cover the shallow modal structure is not a serious problem since the intensity of shallow modal rainfall and its impact on the IVG are small.

As indicated in Table 1, about 15 % of all profiles had peaks as defined above, and most of the peaks were seen above 3 km (87 % for stratiform and 77 % for convective rain). DD trend seems to be significant. More than 70 % of profiles with the peak above 3 km exhibited DD signature. Most of the remaining profiles had a DI signature with

peaks appearing at a high ($\sim$ 5 km) altitude (shown in Fig. 6). For the present study, such profiles were not considered. For example, it was found in the GATE experiment that pre-existing overhang and thick anvil could reach 30 dBZ (*e.g.*, Szoke and Zipser 1986). Most of the peaks at marginally low levels (3 $\sim$ 3.5 km) were DD in nature. The sensitivity of the upper level in the definition of the IVG was checked by mapping the IVG over the globe and comparing adjacent peaks in the histogram profiles (not shown) for various upper levels. DI profiles with marginally low level peaks were embedded sporadically within large rainy regions such as the western Pacific and the highly wet Amazon through the year. It indicates that the adjustment of the upper level for the marginally low level has less impact on final statistics. Most of the gradients with an upper threshold of 4 km increased positively and lessened the number of DD cases. Thus, a level of 3.5 km was retained in order not to deteriorate the detection of peak signals. The IVG is reasonable and proper as an index for a concise but significant characteristic of the vertical gradient of rainfall profiles.

3.4 Characteristics of vertical profiles over Asia

We will focus our attention to the increase or decrease of conditional rainfall-rate profiles around the low level with IVG. We made a $1^\circ \times 1^\circ$ dataset with a simple spatial average. Figure 7 shows the IVG pattern from May to August for all, stratiform and convective rain, respectively. The dark shading indicates negative values of IVG, (i.e., DD). Regarding all rain (Fig. 7, left), DD grids over India and the Indochina region in May and June and over China and the northern part of India in July and August are clearly shown. IVG over the ocean shows positive values, which implies that shallow precipitation dominates. IVG of stratiform rain, (Fig. 7, middle), has a small absolute value and the DD distributes over a wide region covering land and ocean. The weak DD also appears east

(a) stratiform rain

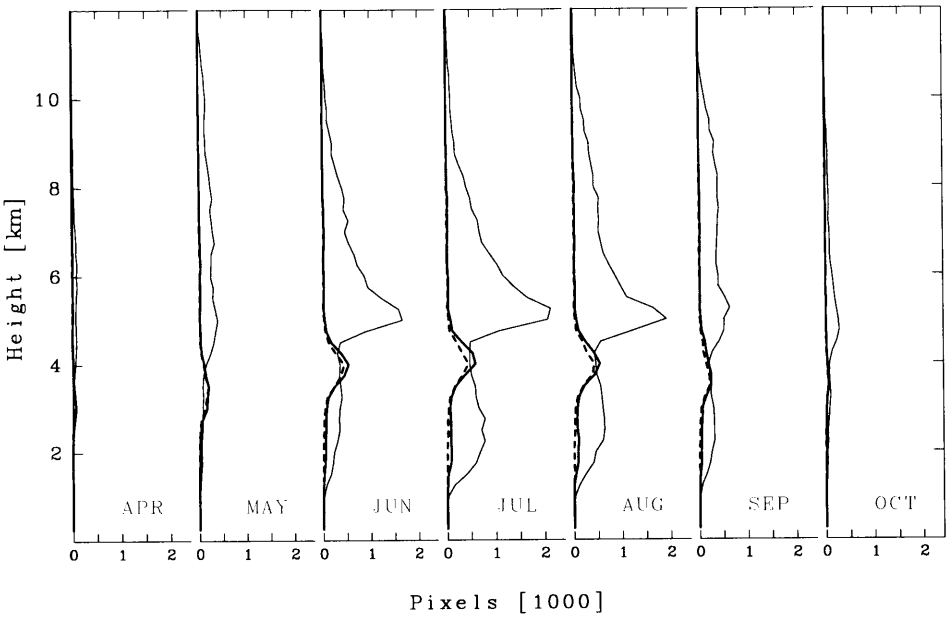

(b) convective rain

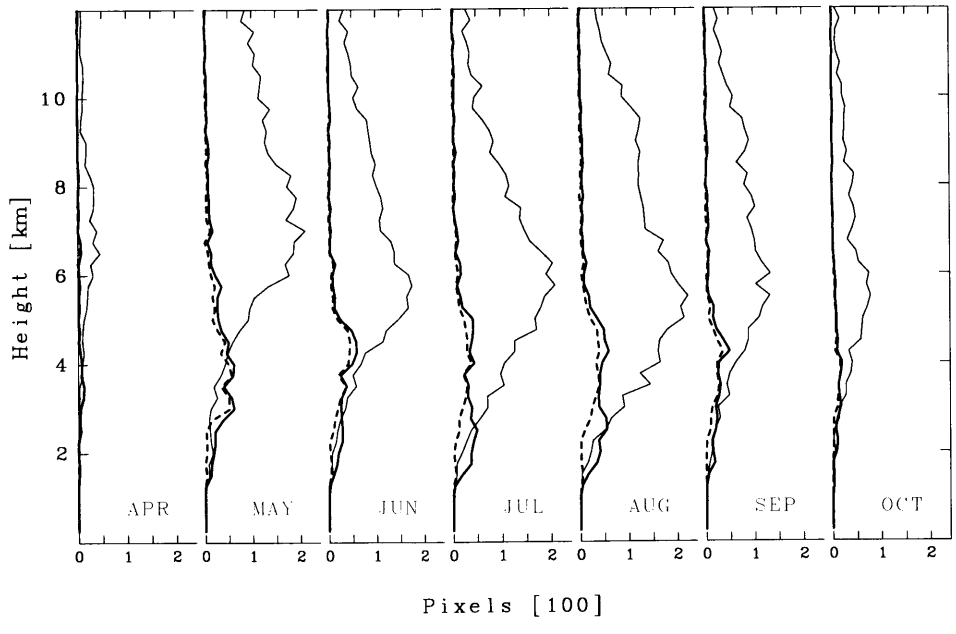

Figure 6. Peak height distribution over inland India from April to October. Thick lines: rainfall rate peak histograms, broken lines: peaks recognized as DD, thin lines: storm height histograms.

Table 1. Ratio of the number of profiles having peaks to all profiles (peak ratio), ratio of the number of profiles having peaks higher than 3 km to those having peaks (high peak), and ratio of the number of peak profiles characterized as DD to those having peaks higher than 3 km (DD peak). The weighted average is shown in the last line. The units are in percentages.

	Stratiform rain			Convective rain		
	peak ratio	high peak	DD peak	peak ratio	high peak	DD peak
APR	23	79	78	17	90	70
MAY	19	90	82	17	85	75
JUN	15	90	78	17	79	76
JUL	13	86	69	17	70	71
AUG	14	86	73	16	71	69
SEP	15	87	70	15	79	68
OCT	9	85	78	14	82	77
Ave.	14	87	74	16	77	72

of India and the South China Sea. We see weak DD and DI in patches over the western Pacific and the eastern Indian Ocean, while DD does not appear around the western Indian Ocean and Arabian Sea. IVG of convective rain, (Fig. 7, right), has a bigger absolute value and the DD distribution is restricted over land. Comparing the change of IVG pattern for all rain with those for each type of stratiform and convective, the DD pattern of all rain is more similar to the convective type rather than stratiform.

The IVG distribution has a seasonal variation. DD migrates northward as the monsoon progresses. The Indian IVG pattern is a notable example. May is before or around onset of the Indian monsoon, and the whole subcontinent is dark shaded (i.e., DD). In June when the rainy area spreads inland, DD over the India subcontinent is conspicuous. The maritime IVG pattern (positive) seems to push the DD region northward over the central parts of India. During July and August, DD decreased over almost all of India except the

northwestern part of India and Pakistan. Rain over a large part of India is substituted by the weak DI pattern. Above this, as the convective pattern indicates, land seems to hinder the progress of maritime DI around the southwestern coastline.

We can also see clear DD over Indochina. The pattern of rainfall is much different from that of India. DD appears around the midpart of the peninsula through a period from May to August. Maritime DI has a clear boundary at the western coast of the peninsula, and the value is nearly 1 mm h^{-1} km^{-1}, which is the same as over India, as shown by the convective pattern. DI does not spread deeply into land like Indian case.

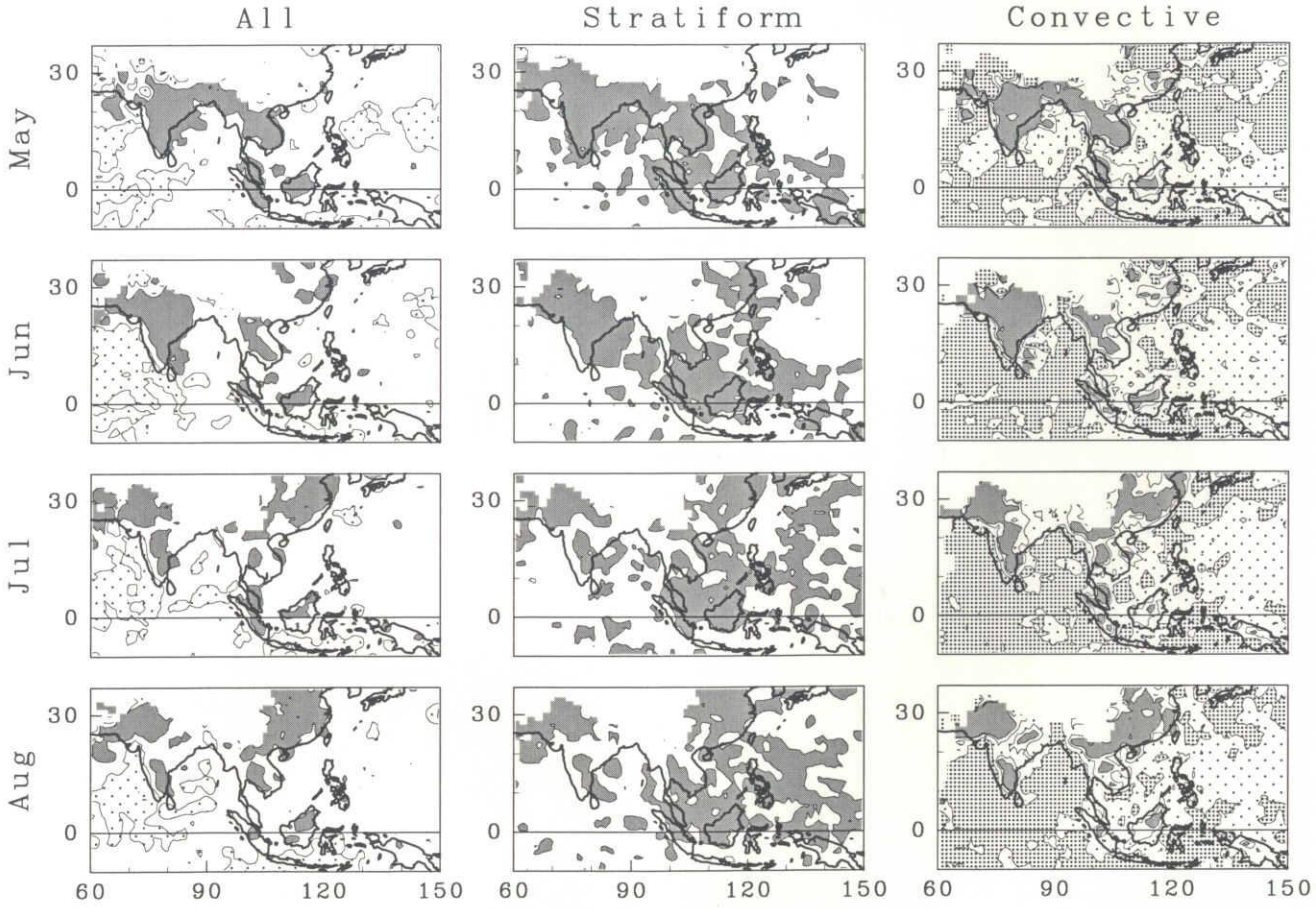

Figure 7. IVG distribution from May to August for all rain (left), stratiform rain (central), and convective rain (right). The dark shading represents downward decreasing. The dotted regions show downward increasing (more than 0.3 mm h^{-1} km^{-1} (coarse dots) and 1 mm h^{-1} km^{-1} (fine dots)). The contours are at -1, 0, 0.3, 1, and 2 mm h^{-1} km^{-1}.

3.5 Seasonal change of vertical gradient

It was described in the preceding section that DD migrates northward as the Asian monsoon progresses. We used 3A25 fine-grid data to investigate the seasonal behavior. In the previous section, we found that the IVG patterns for convective rain represent that for all rain patterns reasonably and that the characteristics are more clear. Since 3A25 does not contain data at 3.5 km height, we used data at 4 km. The conditional rainfall rate at 4 km is still affected by the bright band even during the summer season over most of Asia in the algorithm, although the conditional rainfall rate estimation algorithm is designed to eliminate the brightband effect. Most convective rain does not have a bright band and it shows a similar IVG pattern compared with the 2A25 procedure using rain at the 3.5-km level, while IVG for stratiform rain is noticeably affected by the bright band. Thus, we made IVG using a pair of conditional rainfall rates at 2 and 4 km for convective rain instead of all rain.

We made a latitudinal time section of IVG to investigate the seasonal variation. We produced the percentages of convective DD or DI over land for each latitudinal grid in each month. We calculated the number of pixels of specified IVG divided by the number of rain pixels counted over land. The specification is that IVG is between two thresholds. Here, we used GTOPO30 to distinguish land or ocean for the center of each fine grid of 3A25. We did not use data where the altitude is more than 1000 m (Fig. 8) since the statistics will deteriorate by small sampling numbers due to geographical effects. Figure 9 shows the frequency of occurrence of DD in percentage over Asian land (dark points in Fig. 8). These frequency of occurrences for convective IVG (gray shadings) are calculated for each month using three years of data. The figure indicates that a high frequency of occurrence of DD seems to draw an arc in the latitude-time map from May to October.

The zonal average including rain over non flat land encompasses a large variability of rain patterns. Asia is too large to survey the systematic rain structure which results in DD, considering zonal differences of the monsoon progress over land. Since the migration is most remarkable over India, we will focus on the area (5°–35°N, 60°–90°E), identified as area (I) in Fig. 8. Even over India, we still have spatial variations. For example, rainfall

over the Indian subcontinent is especially concentrated west of the Western Ghats, where the IVG pattern is different from that inland as indicated in Fig. 7. Figure 10 shows the latitudinal time section of monthly rainfall amount (contours) and conditional rainfall rate (shadings) over the western coast (a), inland (b), and eastern coast (c), respectively. The region "coast" is defined as land within 1° from a grid in ocean. Figure 10a shows that rainfall along the western coast is plentiful. In the vicinity of Goa (15.5°N) monthly rainfall is above 700 mm in June and July. Figure 10b represents rainfall over most of the inland region. It shows the typical monsoon type; that is, the rain activity starts in May and June and progresses northward from August to October, then recedes southward. Strong conditional rainfall rate (gray area) is distributed along total rainfall of 50 mm month^{-1} over a large part of India in April and above 30° latitude through monsoon season from May to October. The rainfall pattern over the eastern coast (Fig. 10c) is different from inland one. It shows local characteristics of rain such as plentiful rainfall around Calcutta (22.3°N) over the Bay of Bengal in May and orographic rainfall along the Eastern Ghats in October. The noisy pattern is due to low sampling. The DD migration over India is clear in the map of inland data but not so in the coastal regions.

We exclude coastal regions in order to focus on patterns over land that are not significantly affected by topography. Figure 11a shows the frequency of occurrence of DD over the Indian subcontinent excluding the coastal regions for three years. The contours indicate zonal averaged total rainfall of 50 (dotted line), 100 and 200 mm month^{-1}. The DD region is located over the whole India subcontinent in the wet season. It appears especially around June and September. We see not only the above-mentioned northward migration of DD in monsoon onsets but also a southward withdrawal in the retrogressing periods. It is interesting that DD seems to reduce slightly in the highly wet region and to be bordering the zonally averaged rainfall of around 100 mm month^{-1}. Inside the DD arc, DI regions for less than 1.5 mm h^{-1} km^{-1} are associated with the majority of pixels (light shadings in Fig. 11b). Outside the arc, DI regions greater than 1.5 mm h^{-1} km^{-1} dominate over the dry region (dark shadings in Fig. 11b). These characteristics were seen in each of the three years.

Figure 12 shows the seasonal march of DD with rainfall amount and conditional rainfall rate over India. Clear DD (IVG < -0.5, shadings) concentrates near monthly rainfall of 100 mm (thick line) and is bordering the Indian monsoon. Rain falls infrequently but strongly (5 mm h^{-1}, broken line) if it rains in the premonsoon season. Storm height pattern is similar to one of conditional rainfall rate. Peaks of IVG and conditional rainfall rate or storm height appear in different seasons as sketched in the figure.

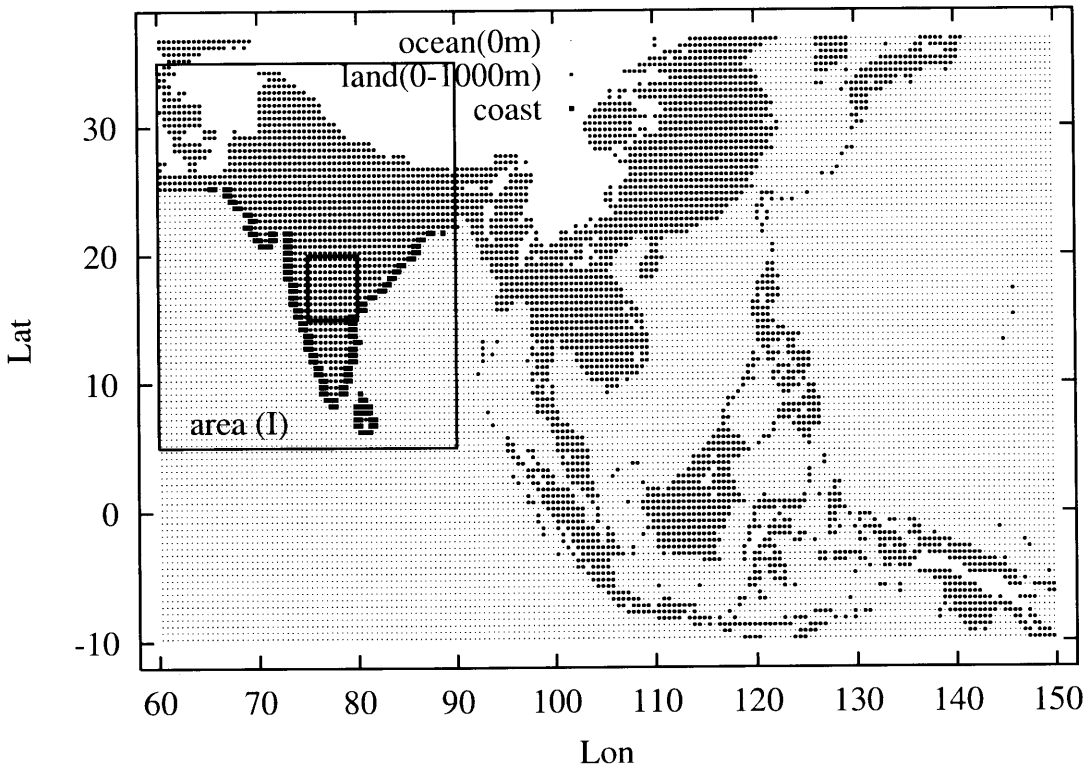

Figure 8. Map of pixels used in zonal average over land and ocean. Dark points indicate land (0–1000 m) and dots indicate ocean. A rectangular area surrounding India ("I") is used for this analysis. Coastline pixels over this domain are shown as black squares and are separated from land. The small box over central India indicates the region for analysis in Section 3.6.

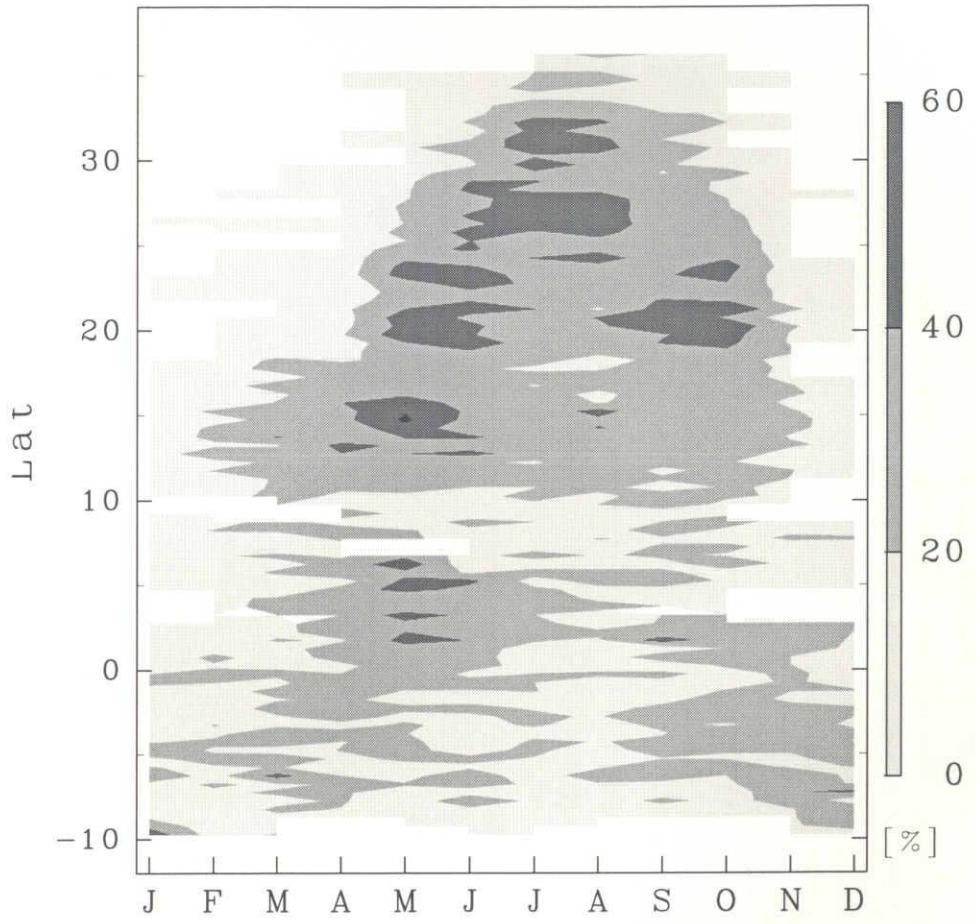

Figure 9. Frequency occurrence of downward decreasing for convective rain over Asian land(10°S–37°N, 60°E–150°E). The shading shows the percentages of IVG which are less than 0 mm h^{-1} km^{-1}.

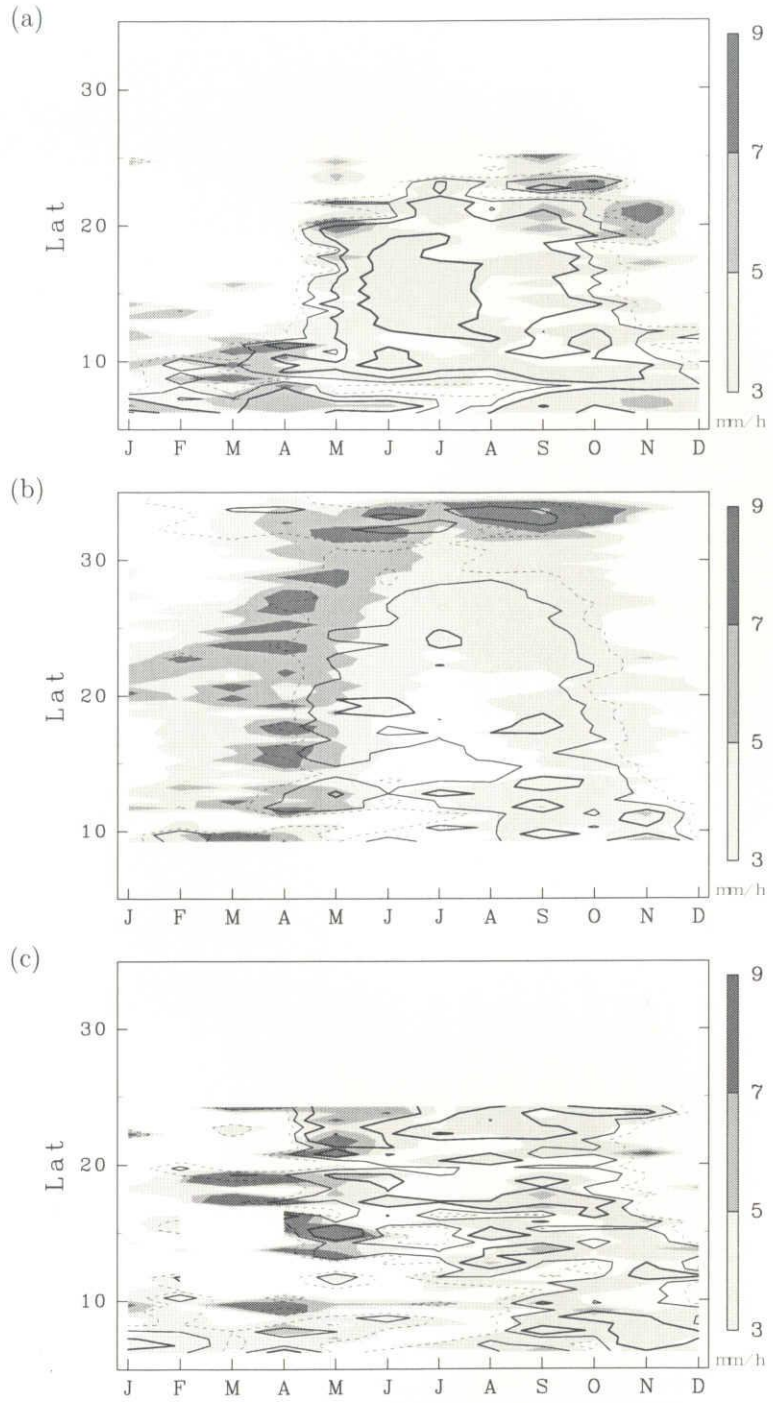

Figure 10. Latitudinal time-section of rainfall amount and strength over the Indian subcontinent (5°N–35°N, 60°E–90°E, area (I) in Fig. 8). Monthly rainfall amount (contours) and conditional rainfall rate (shadings) are averaged zonally for every latitudinal bin of 0.5 degrees width for western coast (top), inland (middle), and eastern coast (bottom). The contours indicate zonally averaged total rainfall. The broken line shows 50 mm month^{-1} and other lines show 100, 200 and 500 mm month^{-1}.

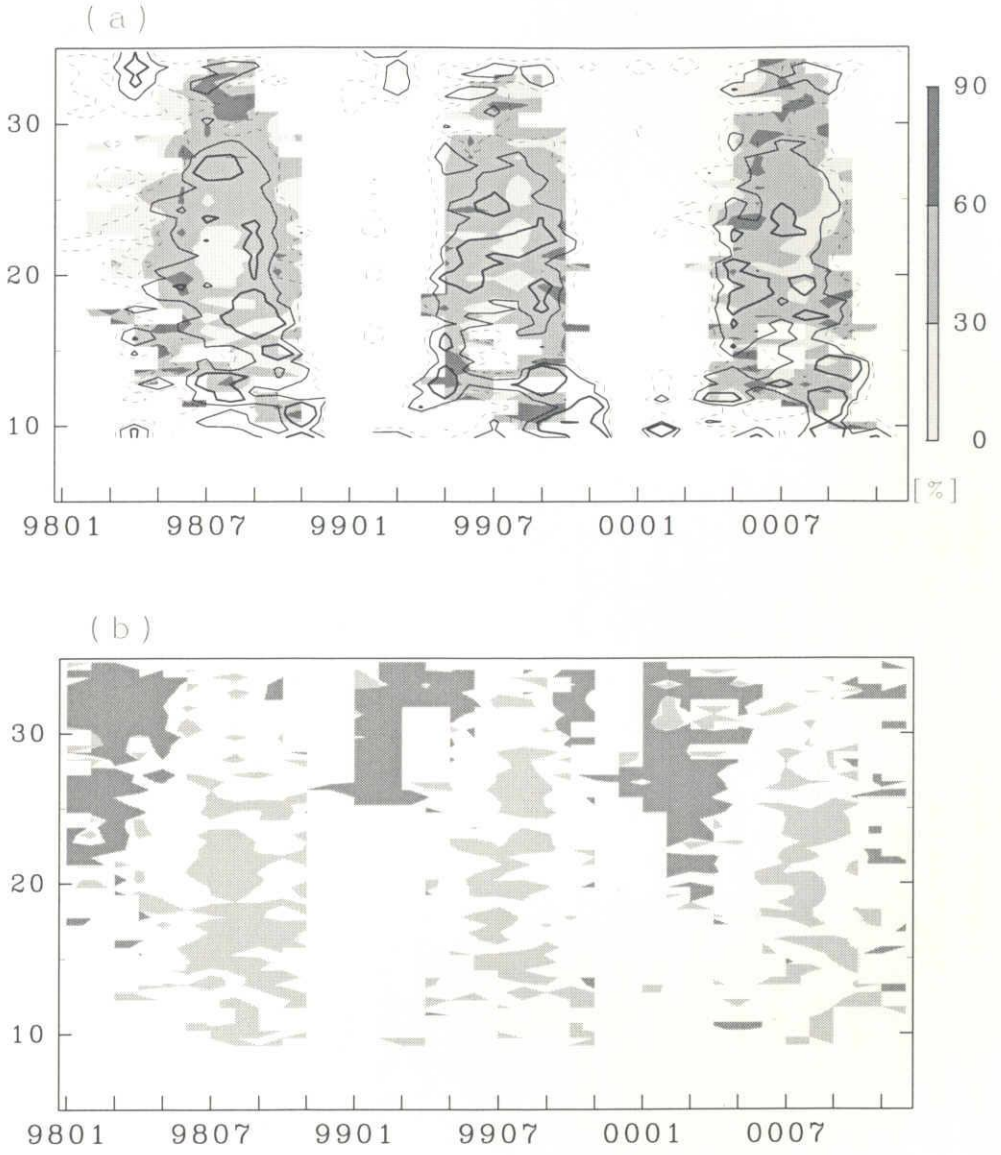

Figure 11. Frequency of occurrence of downward decreasing case (a) and downward increasing case (b) for convective rain over the Indian subcontinent(5°N–35°N, 60°E–90°E, area (I) in Fig. 8) excluding the coast. The contours indicate zonally averaged rainfall. The broken line shows 50 mm month^{-1} and the other lines show 100 and 200 mm month^{-1}. Shadings in upper panel (a) show the frequency of occurrence of DD in percentage. Light (dark) shadings in lower panel (b) show that IVG less (greater) than 1.5 mm h^{-1} km^{-1} has a majority ($> 50\%$).

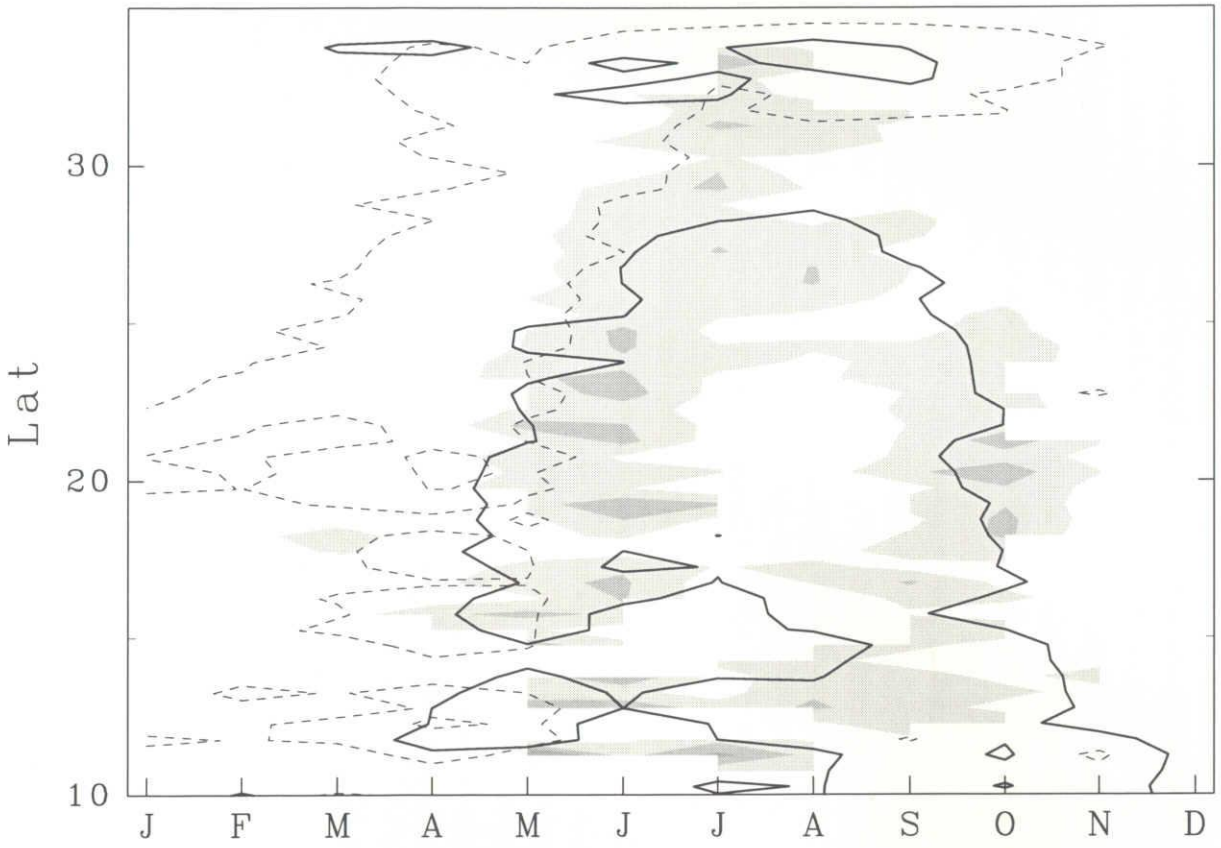

Figure 12. Latitudinal time-section illustrating the relationship between maximum total rainfall (100 mm month^{-1}, thick line), strong conditional rainfall rate (5 mm h^{-1}, dashed line) and clear DD occurrence (IVG<-0.5, light (>20%) and dark (>40%) shadings, respectively) over India. Clear DD occurrence < 20% is not shown.

3.6 Horizontal extent and vertical gradient characteristics over Indian inland region

Here we will examine more details of rain, which results in the above-mentioned characteristics of IVG for conditional rainfall rate profiles. In order to see a relation between IVG and the scale of rain and what contributes to DD, we investigated individual IVG at each pixel with storm height or horizontal extent of rain cells. The analyzed region is over a central part of India (15°–20°N, 75°–80°E) based on 2A25 data.

We looked at monthly averaged rain characteristics over this region (Fig. 13). This figure shows probability of rain, rainfall amount, conditional rainfall rate, averaged storm height, the ratio of DD pixels to rain pixels (DD ratio) and IVG calculated from monthly conditional rainfall-rate profiles for all rain, stratiform rain, and convective rain, respectively. We obtained a storm height here as the highest range bin of three consecutive echoes over 17 dBZ using 2A25 data instead of 2A23. We also compared these monthly averaged data with data for all rain in 3A25 over the same area.

Figure 13a shows the ratio of rain-certain pixels to total pixels. The rain area coverage or probability of rain may be corresponding to a "wet season". We see a clear wet season from May to October and a dry season from November to April. There is a peak almost touching 10 % around August, mainly due to stratiform rain. In the wet season, there is a very small dip around July. This is also seen in Fig. 13b, a time series of monthly rainfall amount at 2 km. Most rainfall over the central parts of India is concentrated in the rainy season during May to October (91 % for three years). The variation of rainfall amount over central India shows a double peak every year, reflecting contributions of strong convective rain. These peaks are shown around May and September and a notable dip is shown around July or August. Stratiform rain also has a slight dip. However, it has no clear peak in May and generally has most rainfall during the mature monsoon. The first peak is dominated by convective rainfall and the second is organized by both stratiform and convective rainfall. The variation of conditional rainfall rate at 2 km (Fig. 13c) resembles that of storm height (Fig. 13d). They have a maximum around the beginning of

the monsoon season and a second peak around the end of the season. Roughly speaking, the 2A25 results agree with 3A25 statistics in the rainy season, while we see differences around March in the dry season. The difference is due to the insufficient sampling of our 2A25 database using narrow swath. We consider 3A25 statistics with sufficient sampling numbers to be reliable, considering the systematic conditional rainfall-rate patterns shown in Fig. 10b. Rain falls strongly in the premonsoon season and during the onset. Storm height seems to be suppressed around 5 km in June, July and August. Figure 13e shows the DD ratio for rain. It gradually increases toward April or May and reaches almost 60 %. After the peak, the ratio is nearly constant from June to September, although we see a very small dip around August. The seasonal variation of DD ratio (Figure 13e) resembles that of storm height. IVG for the monthly conditional rainfall rate profile is shown in Fig. 10f. Roughly speaking, we see DI for the dry season and DD for the wet season. Monthly IVG is positive until April and negative until October and then again positive for November. The variance is large during the dry season due to the small number of samples. Monthly IVG also shows a maximum (weakened tendency of DD) in August during the rainy season from May to October. IVG for convective rain has peculiar variations and has strong DD in May and October, corresponding not to the peaks of rainfall amount or strength but to the beginning and end of the rainy season. These are consistent with the seasonal march of IVG shown in Fig. 11. The rough seasonal pattern of IVG using statistics of 3A25 is similar to that of IVG using 2A25 output, although the IVG was calculated from different data and definitions. However, we should note that IVG using 3A25 becomes larger since a number of peaks in rainfall rate are below 4 km level.

Thus, the peaks of conditional rainfall rate and storm height precede the rainy season. They become weak in the middle of the rainy season and recover moderately at the end. DD frequently occurs in summer monsoon rainfall. It has a primary and secondary peak in the beginning and end of the rainy season. Monthly IVG shows that there are strong DD peaks in the beginning and at the end of the rainy season and IVG becomes larger in August.

Relationships between IVG and storm height for each profile are shown for four

categories of conditional rainfall rate, less than 0.5, 0.5–2, 2–4, and greater than 4 mm h^{-1} in Fig. 14. The contoured frequency by altitude diagrams (CFAD) were made by counting data that fall into 40 (IVG) × 40 (height) intervals in an IVG range between -3 and 3 mm h^{-1} km^{-1} and the height between 0 and 12 km. After that, averaging over 5 × 5 grid was applied to smooth noisy distribution. Light and dark shadings show 1 and 10 per each cell, respectively. Lines indicate monthly averaged IVG with running average over five height intervals. Each line corresponds to one month over three years. The averaged IVG for each level has clear tendencies, while individual IVG values scatter widely. Thick (dotted) lines indicate ones of rainy (dry) season. The thick line showed that the relationship between IVG and storm height is almost steady for all months except for strong and deep storms (Fig. 14d). IVG during the rainy season is a function of conditional rainfall rate around near surface and storm height as a first approximation. It is supported that DD frequently occurs when conditional rainfall rate or storm height is relatively high (3 mm h^{-1} in Fig. 10) during the rainy season in Fig. 12. The relation between IVG and storm height in the dry season seems to deviate from one in the rainy season especially for the strong conditional rainfall rate (roughly, over 4 mm h^{-1}) shown in Fig. 14d, though there exists a large fluctuation due to sampling numbers. For example, the deep storm with a strong rainfall rate in April brings a DI profile. It agrees with the lag seen between peaks of conditional rainfall rate or storm height and the DD occurrence shown in Fig. 12. The relation between IVG and the scale of rain in the dry season differs from the one in the rainy season.

We extended the study into the horizontal scale of rain. Here we took "rain area density" instead of size for the sake of calculatory simplicity. As shown in later chapter, there were similarities between the results using the rain area density and the rain area. First we took 25 × 25 pixels that correspond to around a 100 km × 100 km area. Second we counted the number of rain-certain pixels. Then, we divided the rain pixel number by 25 × 25 to obtain a rain area density. Figure 15 shows the relation between the rain area density and IVG for shallow and deep storms. The thick line designates the averaged IVG for the rain area density. We averaged IVG within ± 10 mm h^{-1} km^{-1} when the sampling

number was more than 10 for each rain area density with an interval of 2 %. The light dots correspond to low storm height (below 4 km) and the dark dots correspond to high storm height (above 8 km).

In the summer monsoon season from May to October, many dots appear, which means that the rainy region covers large areas. IVG slightly decreases as the density increases. For the small area density, DI pixels with low storm height contribute to positive IVG. On the other hand, for high rain area density, DD pixels with high storm height contribute to negative IVG. Rain in large precipitation systems tends to have high storm height and to have a DD profile from May to October. In each month in the dry season, there were only a few rain events during the three years. Storm heights for individual cells do not frequently exceed 10 km in June and July. Numerous DI with small rain percentages contribute more to make the overall DI in the monsoon mature period. We also checked the relationship between rain area density and storm height (not shown). It showed a similar storm height increase with rain area density for each month with deviations of a few kilometers in height. These characteristics of individual rain events are consistent with characteristics of monthly averaged quantities (Fig. 13), although the events have a larger variability.

The results above suggest an image of rain structure over India as shown in Fig. 16. The illustrated large storm implies a wide spreading system covering a large part of the 100 km $\times$ 100 km area, that is, the rain density, instead of the actual horizontal sizes. DD with high storm height is distributed inland around the monsoon onset. Convective rain is dominant. Stratiform rain also shows a DD profile with a smaller slope. In the mature period, DD appears mainly over northern India and the DI profiles of lower and dispersed rain dominate over the rest of India in large parts. The DI-type rain with high storm height around Punjab, the northern part of Pakistan and India (Fig. 2c), is caused by orographic effects. Strictly speaking, it is difficult to interpret literally the position of each stratiform and convective rain.

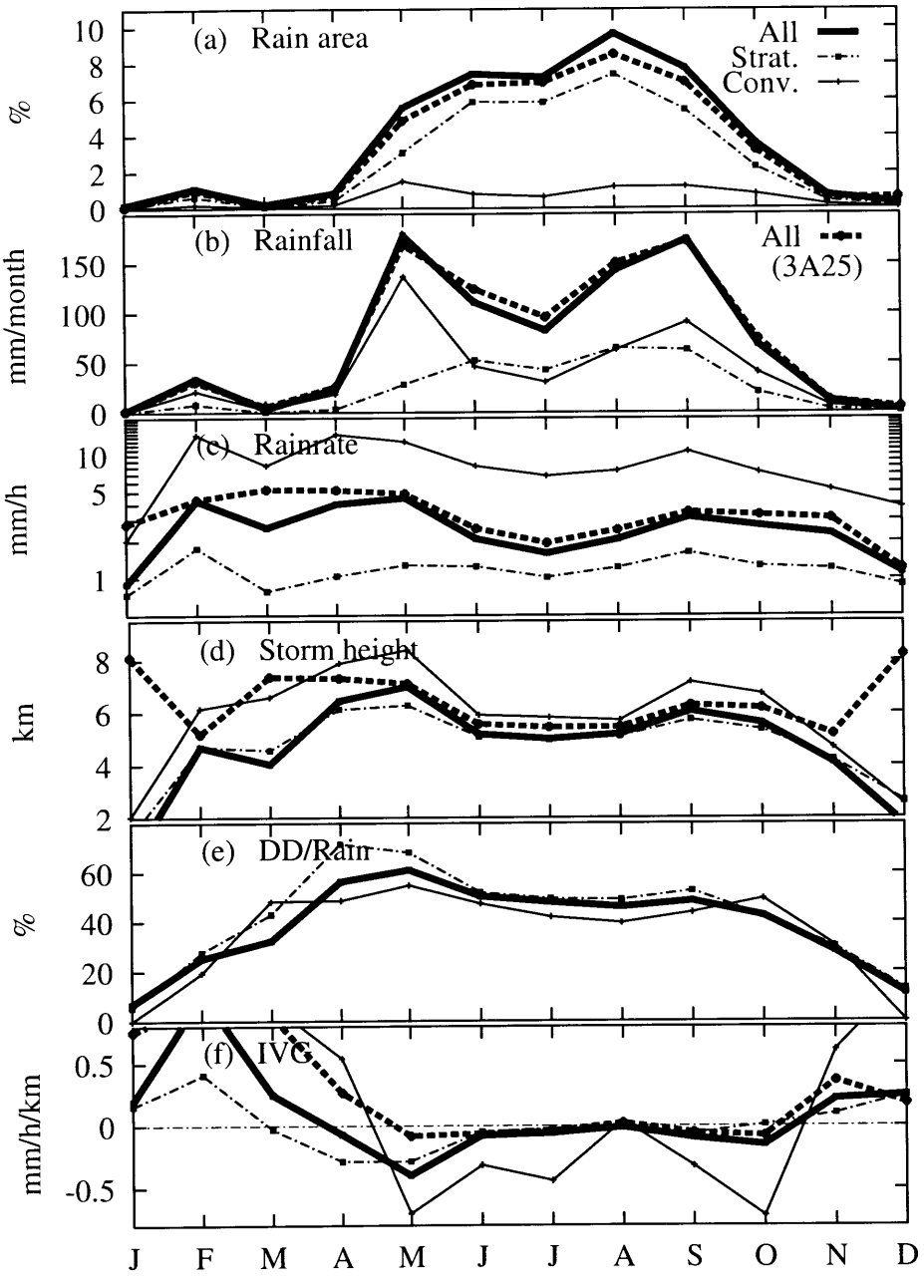

Figure 13. Seasonal variations of the following quantities over central parts of India (15°N–20°N, 75°E–80°E): (a) the probability of rain, (b) monthly rainfall amount at 2 km, (c) conditional rainfall rate at 2 km, (d) averaged storm height, (e) DD percentage for rain pixels, and (f) IVG for the monthly conditional rainfall rate profile. Thick, dash-dotted, and thin lines indicate data using all, stratiform, and convective rain, respectively. Broken line indicates data using all rain of 3A25 over same area.

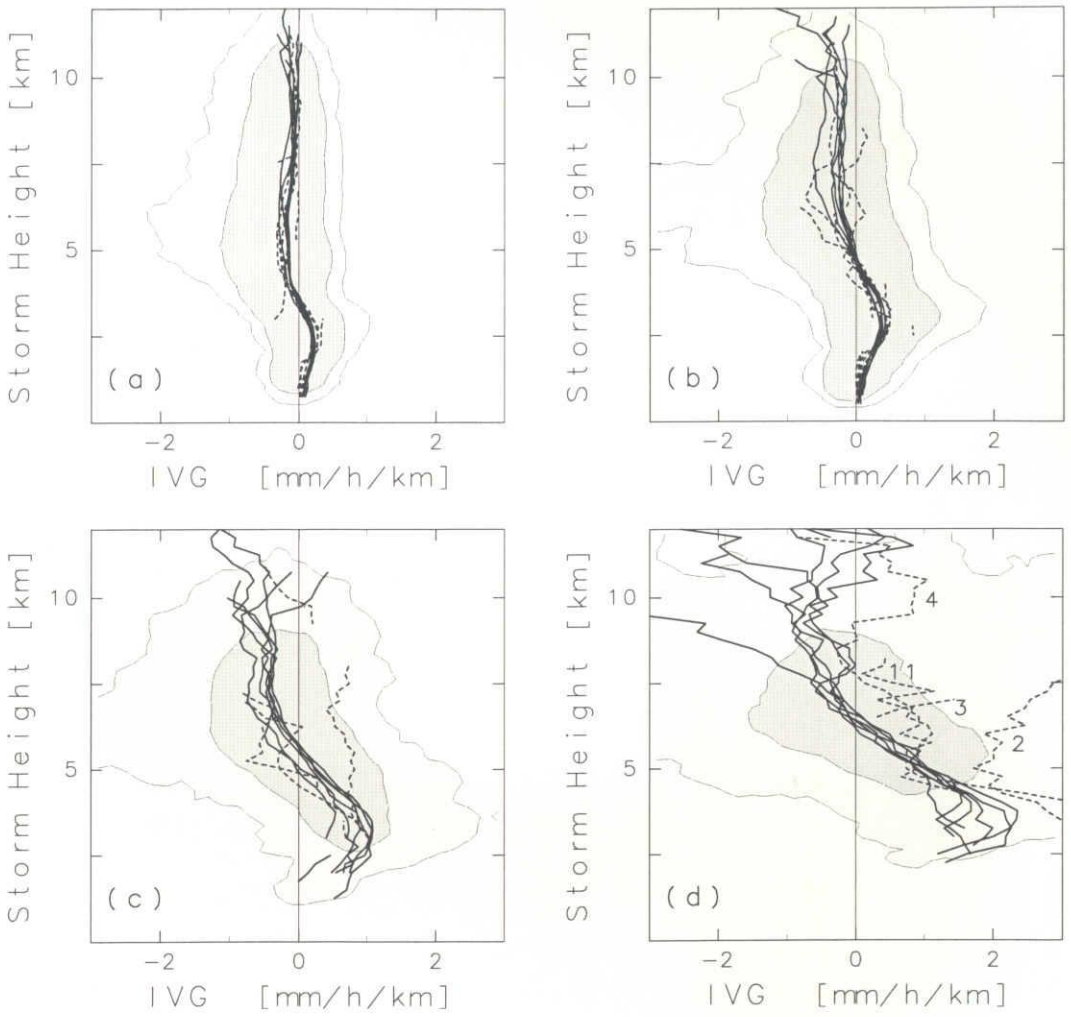

Figure 14. Relationship between individual IVG and the storm height over inland India (15°N–20°N, 75°E–80°E) for the conditional rainfall rate (a) ~0.5, (b) 0.5~2, (c) 2~4, (d) 4~ mm h^{-1}, respectively. Dark (light) shadings indicate high (low) frequency of occurrences. Thick (broken) lines indicate monthly averaged IVG for each storm height of 250 m from May to October (from November to April). The numbers in (d) indicate the month.

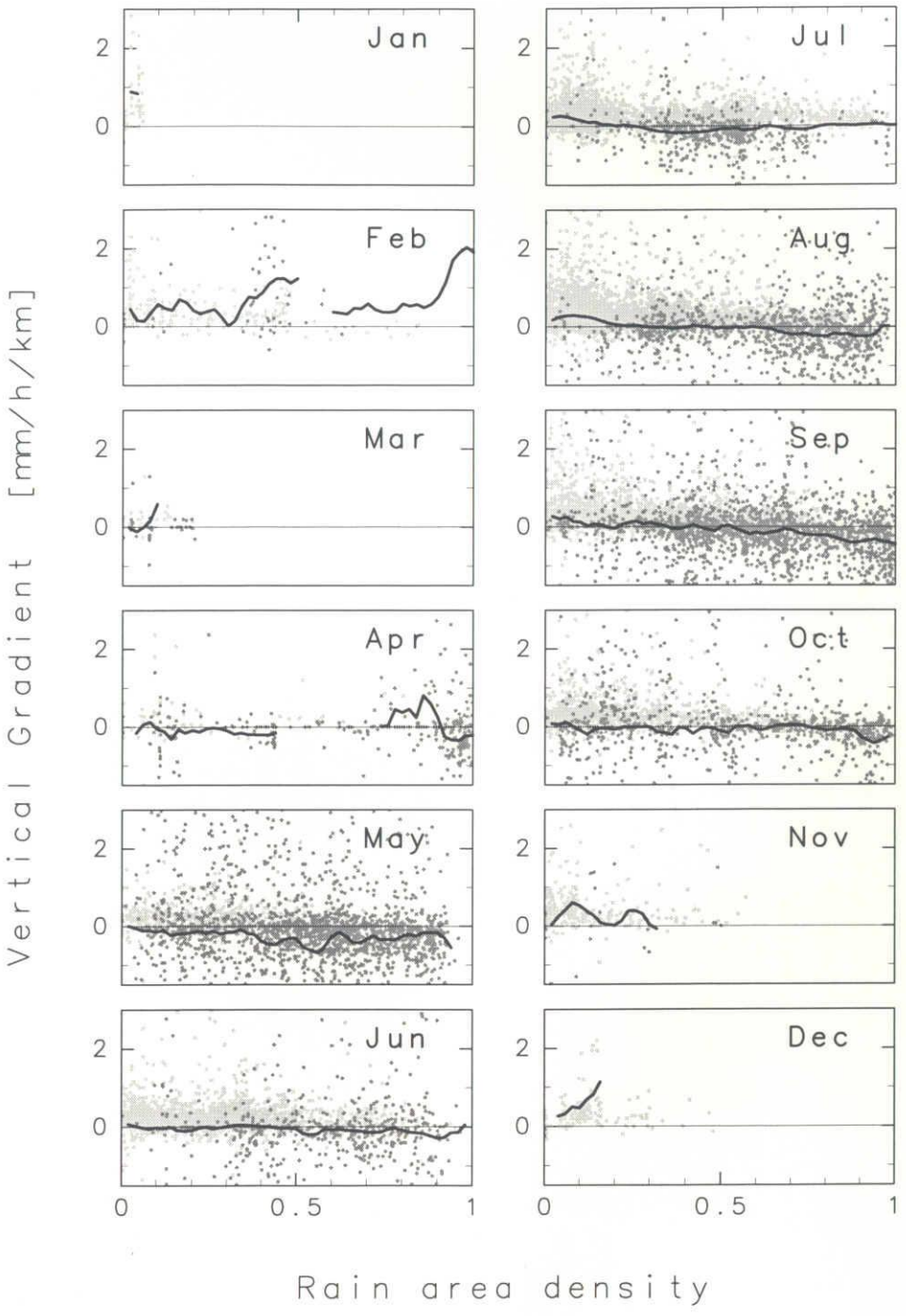

Figure 15. Relationship between rain area density and individual IVG. The rain percentage is obtained over each 25 × 25 footprints correspoinding to around 100 km × 100 km. The data are analyzed over central parts of India (15°–20°N, 75°–80°E). Storm heights are indicated using light (below 4 km) and dark (above 8 km) dots. The thick line shows averaged IVG for 50 intervals in rain percentage.

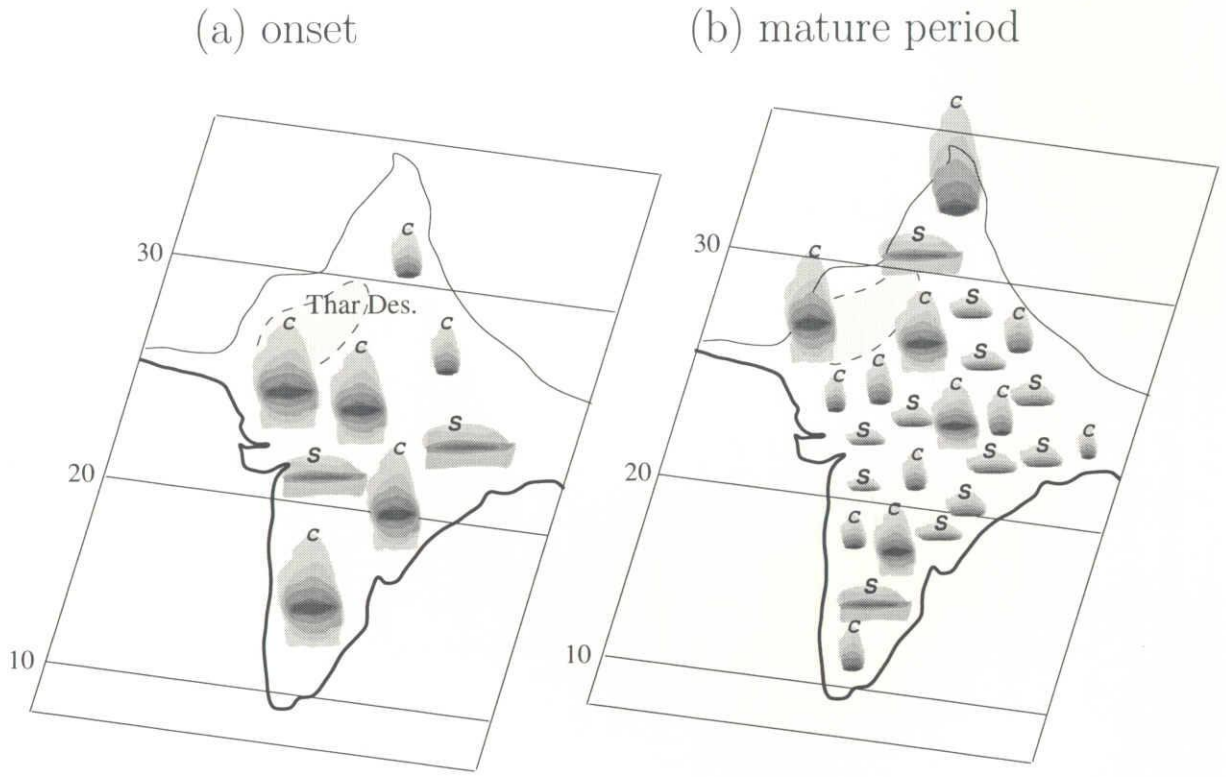

Figure 16. Distribution of precipitation over the Indian subcontinent: (a) monsoon onset, (b) mature period. The character "C" indicates convective rain, and "S" stratiform.

4. Spatiotemporal variation of the vertical gradient of rainfall rate over the global tropics

4.1 Seasonal variation of IVG

4.1.1 Spatiotemporal distribution of IVG derived from monthly mean profiles

We extend the study on the seasonal distribution of IVG over and around India to the global tropics (37°S to 37°N). In this section, we describe the climatological characteristics of IVG. Figure 17 shows the variation of IVG derived from monthly averaged rainfall-rate profiles with $1° \times 1°$ spatial resolution. In general, a significant amount of DD rainfall rates appear over interior landmasses in the summer season. DI rates occur in the winter, in midlatitudes, and over oceans except in regions with very little rainfall. Over Africa, DD dominate throughout the year and are in phase with the rainfall (migrating with the rain between the northern and southern hemisphere). The high frequency of DD rates indicates that tropical interior convective systems have a tendency to be DD in summer. Over India, the northward migration of DD characteristics during the onset of the monsoon and southward withdrawal during retrogressing periods was observed as shown in Chapter 3. Furthermore, DD rates seem to appear frequently between "dry" and "highly wet" regions. This introduces a hypothesis to be considered later. DD rates appear frequently over the Amazon River basin corresponding to the southward migration (August–October) of rainy regions. This is prior to or around the transition period (e.g., September–November), when the convection shows much more continental-like characteristics exhibiting a greater frequency of deep radar reflectivity cores and more frequent lightning (*e.g.*, Petersen and Rutledge 2001; Rickenbach *et al.* 2002). The IVG distribution over this wet region consists of oceanic and continental elements reflecting westerly and easterly flow regimes with

time scales of several days. On the other hand, DD rates widely appear over the Brazilian Plateau. Other regions with significant DD areas are: northern Australia, the Arabian Peninsula, southern plains of the U.S.A., and the Indochina Peninsula. DD profiles over the ocean with very little rainfall (e.g., the eastern Atlantic) had a moderate IVG signature of -0.1 to 0 mm h^{-1} km^{-1}.

The structural differences between significant DD regions over land were examined. The focus being on the latitudinal change of monthly rainfall, rainfall rate and the frequency of occurrence of DD profiles. The following regions were highlighted: the African continent having a typical continental-like pattern, India characterized by abundant monsoon rainfall, and South America which includes the wet Amazon region and the wet or dry Brazilian Plateau. Figure 18 shows the latitudinal and temporal variation of monthly rainfall, strong rainfall rate (> 4 mm h^{-1}), and DD occurrence over the regions described above. A significant fluctuation in rainfall north and south of the equator with an amplitude of about 10 to 15 degrees in latitude is observed over Africa (Fig. 18a). The significant DD region does not overlap the maximum rainfall region. The horseshoe-like pattern in Fig. 18b is almost identical to Fig. 12 but only for convective rain. DD characteristics are slightly reduced in the highly wet region and instead coincide with the zonally averaged rainfall contours of around 100 mm $month^{-1}$. Strong zonallly-averaged rainfall rates were observed over India in the premonsoon season and in the northern part of India and Pakistan in mid to late summer. Most of the significant DD pixels correspond to relatively strong rainfall rates (> 3 mm h^{-1}, Fig. 10b). There are similarities between the rainfall over Africa and India. The highest DD occurrence is located on the fringe of the large rainfall amounts. The amplitude of the sine-curve pattern of DD occurrence is larger than that for the rainfall amount. The occurrence of DD profiles over India is synchronized with the pattern over Africa. There are, however, several significant differences between them. The most significant one being that the pattern over India does not have a maximum frequency of occurrence of DD profiles around 15°N in the middle of summer that overlaps with the mature phase of the monsoon. The rainfall over Africa can be classified as "continental" considering the sine-curve pattern of DD characteristics that correspond to the maximum

heating by solar insolation. In addition, the variation of moisture inflow from the ocean can be crucial in changing the structure of tropical interior convection over India.

Rainfall over South America, mainly Brazil (Fig. 18c), also has such similarities with the other rainy regions. One of the main characteristics is the northward migration of extensive rainfall regions with DI profiles around the Amazon River basin. These oceanic characteristics are consistent with earlier results (*e.g.,* Garstang *et al.* 1994; Schumacher and Houze 2003a). DD profiles appear widely before and around the transition period of the South American rainy season as mentioned above. The region from 10° to 20°S (mainly over the Brazilian Plateau) was generally characterized as DD. The strongest rainfall rates, on average, were found particularly around 30°S corresponding to the Pampa Humeda.

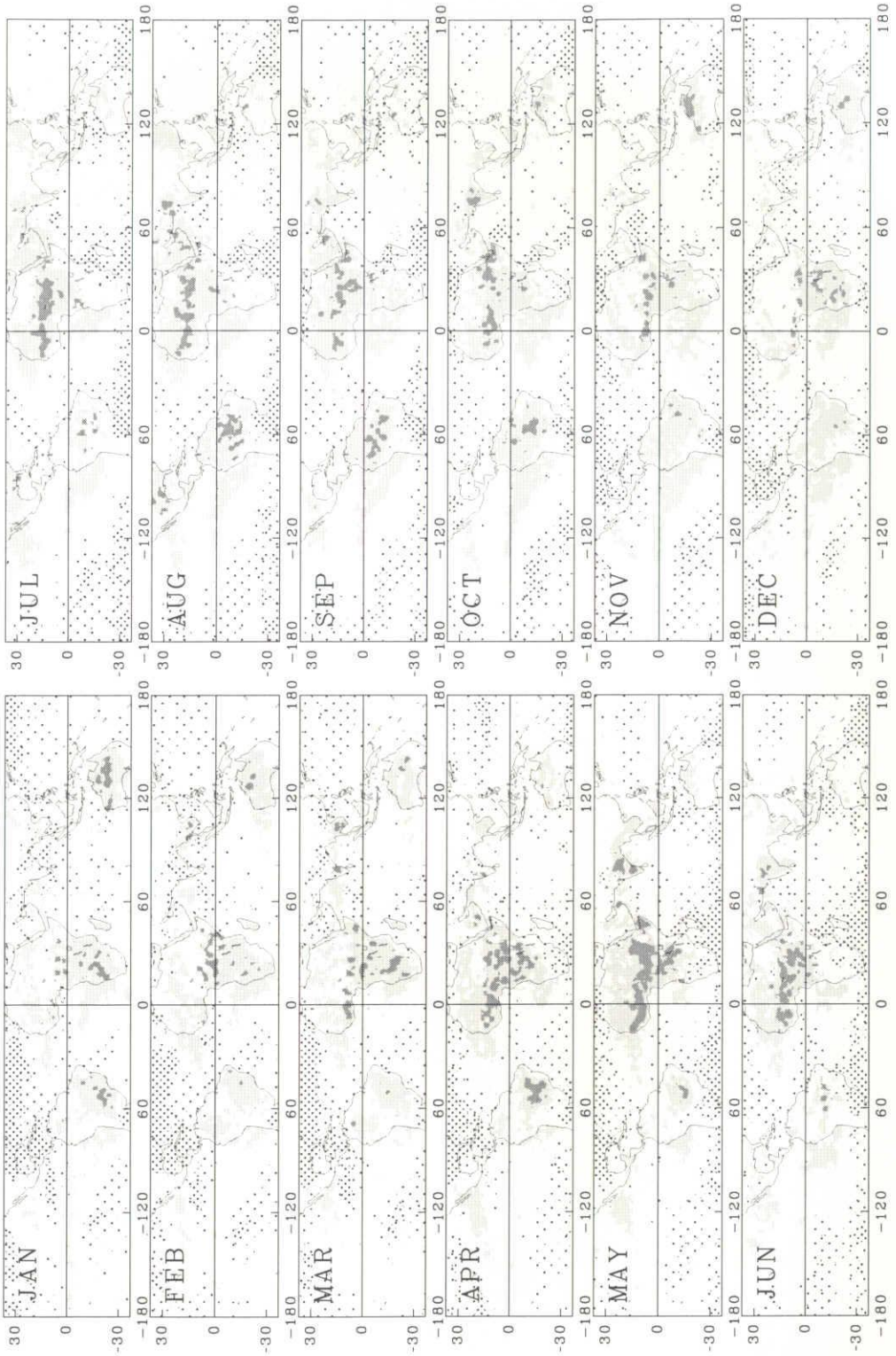

Figure 17. Monthly IVG map over the global tropics. The spatial resolution is 1°× 1°. Dark (light) stipple indicates significant DI: 0.6 < IVG (moderate DI: 0.3 < IVG < 0.6). Dark (light) shading represents significant DD: IVG < -0.3 (moderate DD: -0.3 < IVG < 0).

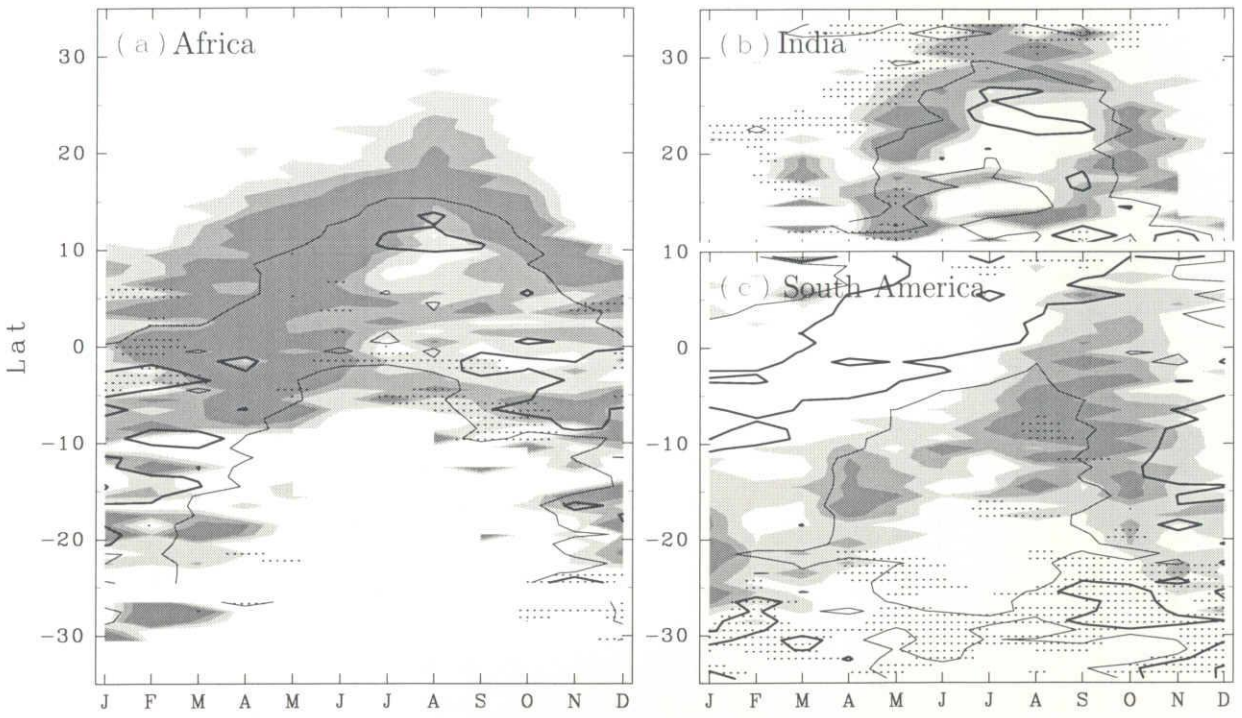

Figure 18. Latitudinal time-section illustrating the relationship between monthly total rainfall (100 and 200 mm month^{-1}, thin and thick lines), strong rainfall rate (4 mm h^{-1}, dotted regions) and strong DD occurrence of IVG<-0.5, gray shading (10–20 %, 20–30 %, and more than 30 %) over (a) inland Africa (20°W–50°E), (b) India (60°–90°E), and (c) South America (80°–40°W).

4.1.2 Variation of IVG in differing moisture environments

The variation of IVG with atmospheric conditions is examined in this section. Monthly and latitudinal variation of the frequency of occurrence of DD profiles over India showed a one-to-one correspondence with storm height, the mean number of thunderstorm days, and the mean maximum surface wet-bulb temperature. (Manohar *et al.* 1999). In addition to the systematic changes in the equatorial convective zones, dry and wet regimes are also of interest. Trenberth (1998) showed relationships between wind, precipitation, and atmospheric water vapor with a recycling ratio and reported that precipitation associated with transported water vapor dominates in the monsoon onset period, while precipitation associated with evaporated and recycled water vapor dominates in the late or post-monsoon season. Several climatological elements such as moisture inflow, surface soil moisture, and evapotranspiration from vegetation do not correspond with DD occurrences that show relatively symmetric succession between the onset and the retrogressing periods, while variations in the surface boundary may affect significantly subsequent convective systems.

To explain the change in precipitation-system structure associated with wet and dry environmental conditions, knowledge of the amount of atmospheric moisture is helpful. Figure 19 shows the effect of total water vapor on IVG over India, northern Africa, the Amazon River basin, and the Brazilian Plateau. The area of these locations is approximately 1.1×10^6, 8.8×10^6, 1.3×10^6, and 3.5×10^6 km^2, respectively. The inland regions were selected as either DD-significant regions or highly wet regions affected by moist maritime air. The abscissa shows precipitable water derived from NCEP/NCAR reanalysis data (Kalnay *et al.* 1996; Trenberth and Guillemot 1998) and the ordinate average rainfall rate derived from the TRMM PR with a 2.5 degree resolution.

Comparing India (5°–25°N, 65°–90°E) and northern Africa (10°–25°N, 20°W–50°E) shows the difference in water vapor amount and the affected precipitation-system structure in IVG. A DD signature dominates in summer over these regions as was expected. In other words, DD appeared from April or May to October when precipitable water is below 50 mm. On the other hand, DI profiles appear during winter when precipitable water is relatively low. In mid summer when atmospheric water vapor was around or more than

50 mm, the rainfall rate weakened and had DI characteristics over India. Since water vapor amount is a maximum in August, the lower atmosphere gets saturated (*e.g.,* Ninomiya and Kobayashi 1998; Lim and Kim 2002). The relative humidity in mid to late summer is $\geq$ about 80 % at 850 hPa (not shown). At the height of the wet season, precipitation and cloud (*e.g.,* Laing and Fritsch 1993b) are at a maximum reducing the solar insolation at the surface. The abundance of water vapor turns the continental precipitation regime into a quasi-oceanic one. In other words, the monsoon brings highly moist air into inland India. As a result, DD profiles, which typically border the monsoon rainfall regimes, are deemed to be located where there is more moderate amounts of water vapor.

The study area over northern Africa includes two distinct precipitation regimes: the northern desert/steppe region and the tropical savanna region. This is evident in the distribution of precipitation as many large systems are concentrated around 10°–15°N with few systems around and north of 20°N (not shown). DD profiles with weak rainfall rates and low atmospheric moisture in the summer months are mostly observed north of 15° N. All regions over northern Africa had lower atmospheric moisture than over India and showed a DD tendency during the mature summer. The elevation of the inland Amazon River basin is less than 100 m (10°S–5°N, 80°–50°W). The precipitation regime is similar to that over India during the wettest part of the summer. The monsoon/tropical rainforest has abundant water vapor (40–55 mm) resulting in DI profiles from January to June, predominantly in April and May. In contrast, atmospheric moisture over the Brazilian Plateau (30°–5°S, 60°–35°W, elevation of 200–1000 m) is less. DI signatures associated with abundant atmospheric moisture are less. Most of the region remains DD during the rainy season. Even in winter, the atmospheric moisture and DD fraction is higher than those over India and Africa. These results suggest that the IVG in dry winter, wet summer, and highly wet summer is DI, DD, and moderately DI, respectively.

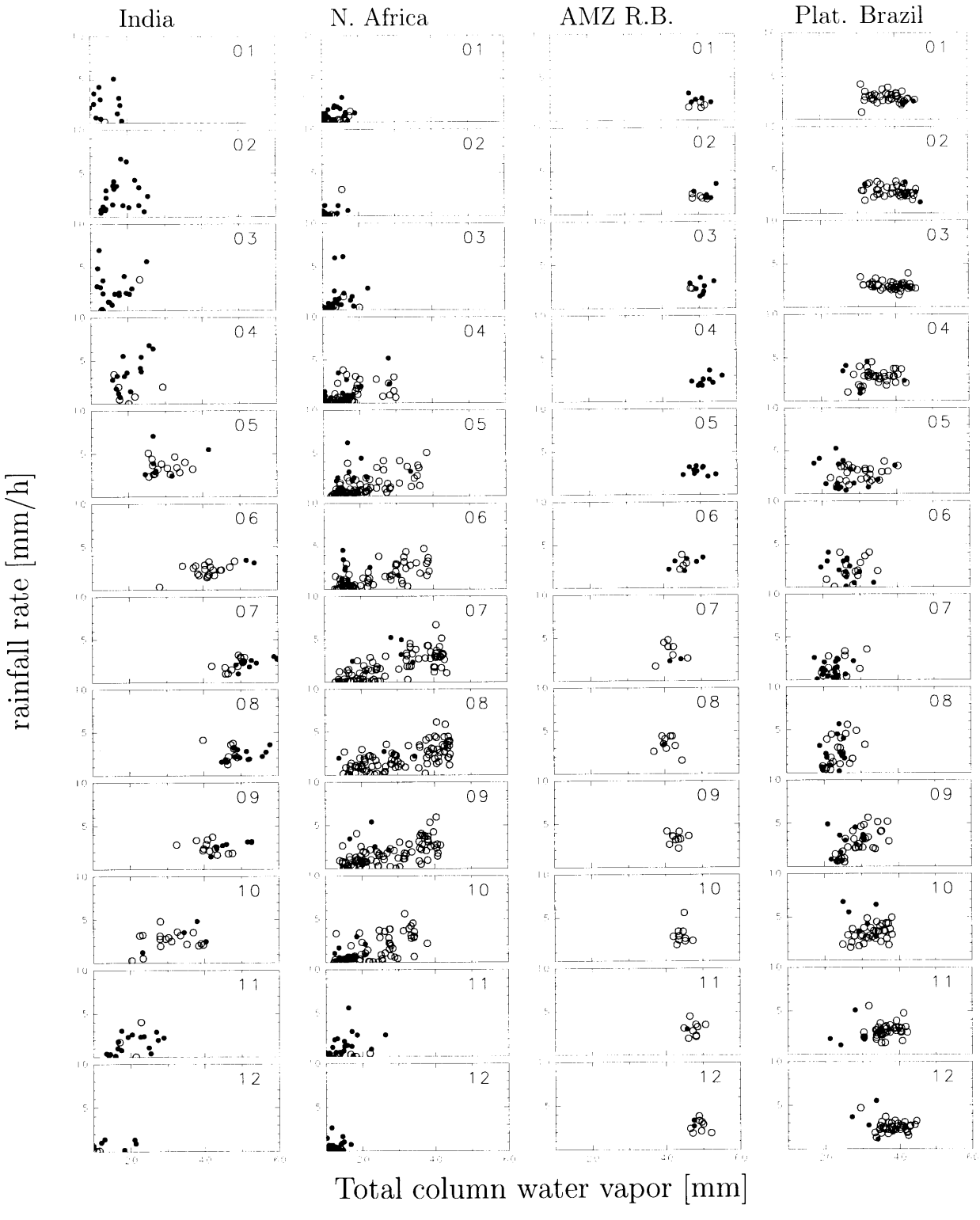

Figure 19. Regional difference relationships between DD and DI, total column water vapor, and rainfall rate at 2.5 degree spatial resolution. Circles and dark points represent DD and DI. Shown are central and southern India (10°–25°N, 65°–90°E), northern Africa (10°–25°N, 20°W–50°E), the Amazon River basin (10°S–5°N, 80°–50°W, altitudes of 0–100 m), and the Brazilian Plateau (30°–5°S, 60°–35°W, altitudes ranging from 200 to 1000 m).

4.2 Vertical characteristics of individual rainshafts

Individual rainfall-rate profiles can be characterized by the storm height, the rainfall rate near the surface, and the vertical gradient at low levels. The main area of interest is India where the IVG transitions through a change of dry, wet, and highly-wet seasons. The rainfall over inland India has been characterized in terms of IVG and rainfall rate (Fig. 18b). Figure 20 shows a schematic diagram of precipitation over inland India in terms of four phases: the winter period (phase A), the hot season prior to the monsoon (phase B) with significant DI profiles (a majority of the IVG greater than 1.5), a DD-salient phase (phase C) surrounding the highly wet monsoon region, and the mature phase of the Indian monsoon (phase D) dominated by moderate DI profiles (a majority of the IVG between 0 and 1.5). The IVG shows significant variation with time in the region (i.e., south of 25°N). In Chapter 3, we found that DD profiles generally represent deep storms and DI ones shallow storms. Further, it was found that the general relationship between IVG and storm height for the rainy season may not be valid for the premonsoon season when significant DI profiles were present with high storm heights and strong rainfall rates. These variations suggested the necessity for further investigation.

Figure 21 shows the relationship between near surface rainfall rate and storm height for DD and DI stratiform and convective rain profiles in each phase from A to D as defined in Fig. 20. IVG is averaged over each grid (50 (rainfall) $\times$ 80 (height) intervals) and the number of profiles in the grid are shown as contours and shading, respectively. Crosses/circles indicate individual profiles with a significant DD/DI (i.e., IVG $> \pm 30$). The stratiform rain patterns show that moderately high storms having moderate DD profiles and low storms having moderate DI profiles generally form the monthly IVG. Below 5 km, DI profiles dominate the winter. As the season progresses, moderately high storms with moderate DD profiles increase and reach a maximum number in summer. Simultaneously, DI profiles associated with low storm heights of a few kilometers appear mostly in weak rainfall rates. DI profiles in low storm heights also existed in the case of convective rain profiles. A striking difference between the two types is the difference in magnitude of the

significant IVG. In winter (phase A), most of the precipitation is associated with moderate DI signatures and some moderate DD profiles for mid-level heights. In the premonsoon season (phase B), heavy rainfall (> 50 mm h^{-1}) that is mainly DI dominates. At the start of the rainy season (phase C), deep convective storms reaching up to 15 km with significant DD signatures and strong rainfall rates are noticeable. Monthly averaged rain profiles in this phase are DD every year in spite of the existence of some significant DI profiles. Similar features are present in the postmonsoon season. At the height of the wet season (phase D), precipitation associated with a high IVG, strong rainfall rates, and deep storms disappears. This mode seems to be suppressed and changed into a monsoonal rain with moderately low storm heights, weak rainfall rates, and moderate IVG.

As a whole, shallow precipitation noticeably increases in summer. Storms higher than about 5 km have a tendency to be DD with the deepest ones (> 15 km) strongly DD (IVG < -10 mm h^{-1} km^{-1}). Rainfall rate, storm height, and IVG are well correlated in DI profiles; the stronger or deeper the storm, the stronger the DI gradient. Rainfall exceeding 50 mm h^{-1} was often associated with significant DI profiles (IVG > 30 mm h^{-1} km^{-1}). It is plausible since an IVG of 30 mm h^{-1} km^{-1} is equivalent to a rainfall-rate change of 45 mm h^{-1} between 2 km and 3.5 km. However, there were a few exceptional cases with weak rainfall having significant DI profiles. For example, there was a profile with a near-surface rainfall rate of 9.0 mm h^{-1}, a storm height of 12.75 km, and an IVG of 30.5 mm h^{-1} km^{-1} (convective rain in May). After careful inspection of the horizontal pattern (not shown), it was located at the edge of a mesosale convective system and was part of an organized three-dimensional structure and will be discussed later. The profile had a maximum of 74.1 mm h^{-1} at 2.5 km and a sharp decline from 2 km to 1 km.

The above procedure was used to study IVG characteristics in other regions as shown in Fig. 22. The first panel (top left) is for convective rain over northern Africa (10°–25°N, 20°W–50°E) in August, which corresponds to the most significant DD region. It shows significant IVG characteristics more clearly than those observed over India and Africa in May (not shown). The number of significant DD profiles was higher for those with storm heights of 15 km and a near-surface rainfall rate of 50 mm h^{-1}. Deep storms

with strong rainfall rates had significant DD profiles accompanied by significant DI profiles. The pattern in March over India did not have significant DD profiles but only significant DI ones. Such precipitation regimes shown in phase B, did not appear over northern Africa. This will be examined later by looking at precipitation systems as a whole. The second panel (top right) is for convective rain around the Amazon River basin in September during which DD signatures dominated. The observed pattern is similar to the one over India during phase D with a few significant IVG cases. The fraction of DI is less.

The lower two panels in Fig. 22 show oceanic cases. In general, monthly profiles of oceanic rainfall are characterized by low storm heights, weak rainfall rates, and DI profiles. Rainy regions that contain deep storms have a smaller IVG but are still DI (Fig. 7). The third panel (bottom left) shows convective rain over the South China Sea in August and corresponds to the active regions of rainfall. The fraction of shallow storms that are moderate DI is larger than the storms that are moderate DD, in contrast to the cases over land shown in the top panels. Despite the similarity in the relationship between near-surface rainfall rate and storm height, characteristics of the IVG are in striking contrast for these different precipitation regimes. The last panel (bottom right) is for all precipitation over the eastern part of the South Atlantic Ocean (off the coast of the Republic of Angola) and is typical of a region with very little rainfall (6.8 mm year^{-1} near surface) over the ocean. This region is located on the eastern edge of the Atlantic high and over the cold Benguela current with strong up-welling. Storms were separated into two groups based on altitude. Atmospheric subsidence appeared to be closely associated with the shallow storms around and below 2 km. Short and Nakamura (2000) reported that this is one of the regions where, on average, the shallowest precipitation falls. The small number of DI profiles is an important characteristic of this type of light, oceanic rainfall. The second group appears at and above 5 km and has DD characteristics. Isolated DD profiles constantly appear all through the year. The bi-modal structure or capped height around 2 km and 5 km is widely seen over oceans (Short and Nakamura 2000). However, the rainfall and the fraction of DI profiles are smaller than in other oceanic cases having bimodal structure.

In order to understand the above-mentioned profile characteristics, analyses for

each system as a whole will be done over landmasses in the following section. Here, the horizontal extent of rain area as defined in Chapter 2 is introduced to understand the oceanic profiles with very little rainfall. There were 7758 systems in the region during the three years, and the vast majority of them (97 %) were small with rain areas < 100 km^2. Sixty six percent of the 4567 DD profiles and 79 % of the 6070 DI profiles were embedded in these isolated small precipitation systems. During the three year period, the largest observed system was 9090 km^2 and contained 60 DD profiles and 27 DI profiles. The small number of DD and DI profiles was mainly due to the restriction of the calculation of IVG in a narrower swath and the existence of other types. Over other regions, large systems were dominant. For example, 68 % of the DD and 49 % of the DI profiles were embedded in a few (3 %) but large ($> 10^4$ km^2) systems over the South China Sea. Weak precipitation systems over the ocean with very little rainfall are most likely related to the climatological conditions there. Precipitation over the ocean with very little rainfall can be classified into two types based on IVG, i.e., isolated shallow and weak storms with DI profiles and moderately high but isolated and weak storms that are DD. However, the actual number of small weak events does not give an accurate proportion (Chapter 2). The 2A23 version 5 algorithm classified almost all of this rain as "stratiform". These isolated rainfall systems should be interpreted as shallow, warm convective rain (Heymsfield *et al.* 2000; Short and Nakamura 2000; Schumacher and Houze 2003b).

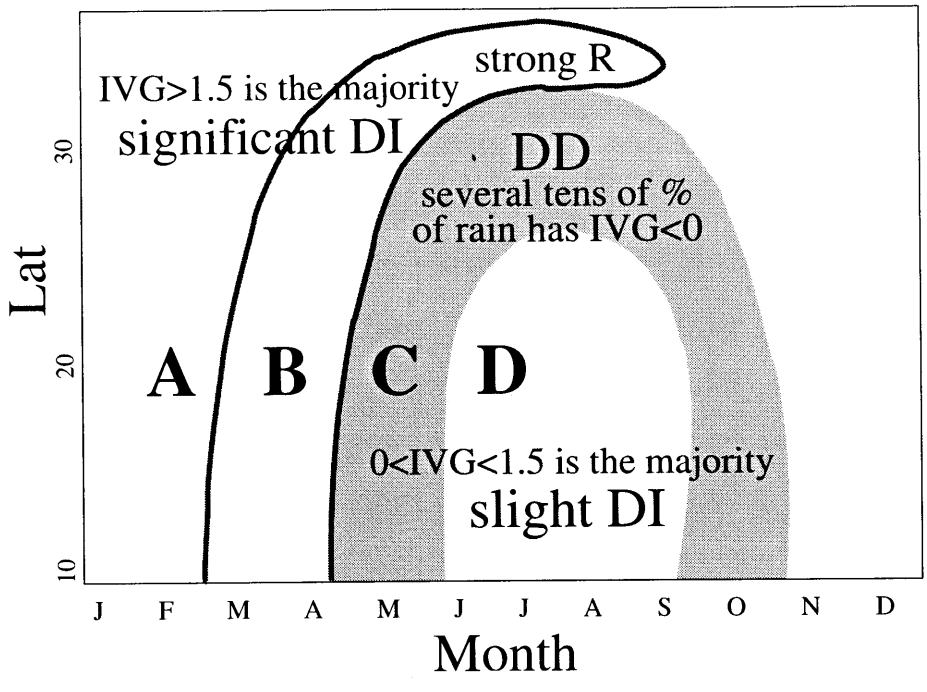

Figure 20. Schematic diagram for seasonal and zonal mean precipitation structure over inland India. Abscissa and ordinate are the same as in Figure 18b. A, B, C, and D indicate the phase characterized by IVG and rainfall rate.

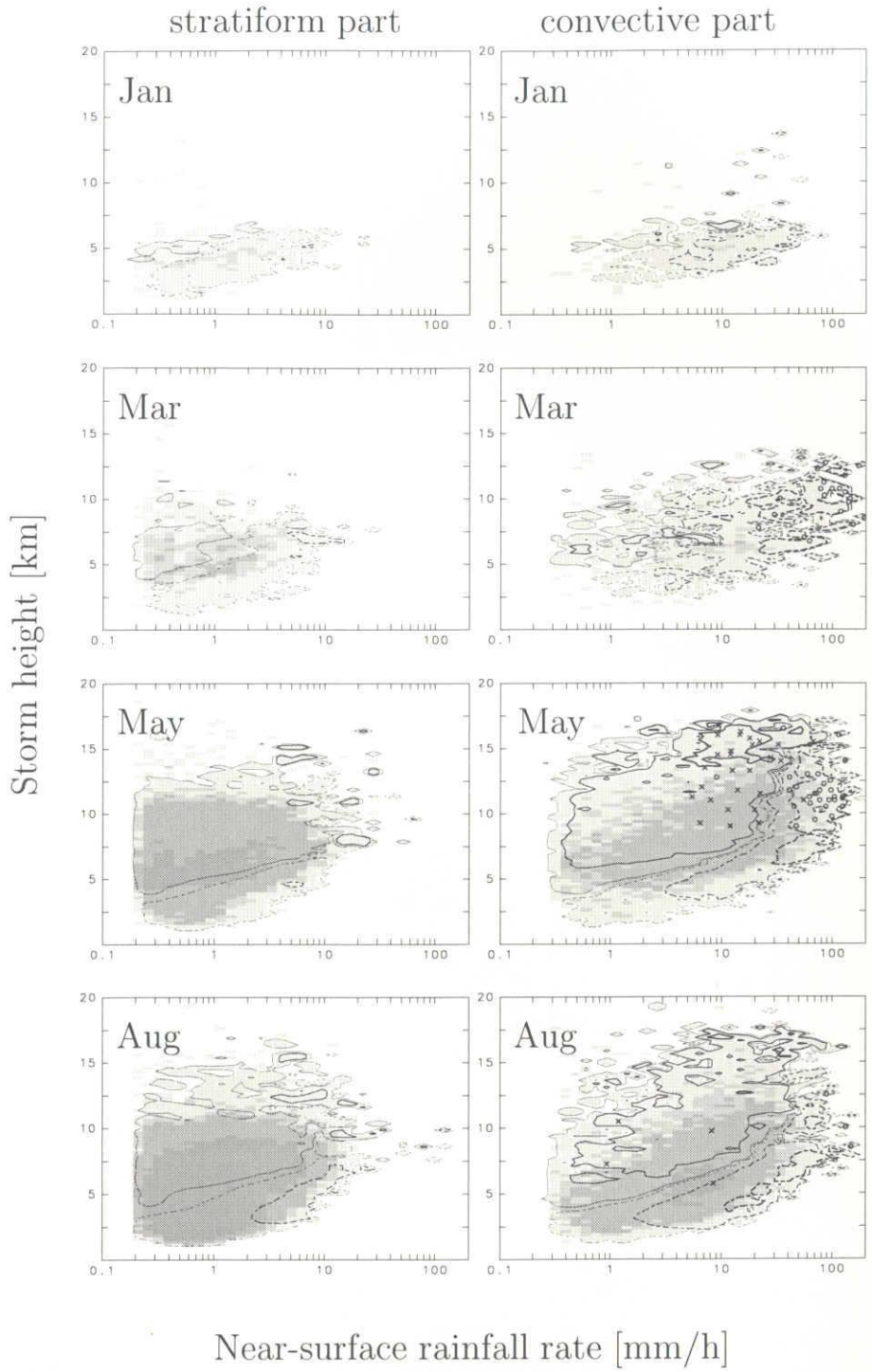

Figure 21. Relationship between rainfall rate, storm height and IVG for individual rain profiles over inland India. Rain in January, March, May, and August is depicted as typical of phases A to D in Figure 20 for stratiform (left) and convective (right) rain, respectively. The shading indicates sample numbers of 1, 5, 10, and 50 over each grid which fall into 50 (rainfall) × 80 (height) intervals in a rainfall rate range from 0.1 to 200 mm and heights between 0 and 20 km. The solid (dashed) lines indicate DD (DI). The contours indicate an IVG of -5, -1, -0.1, 0.1, 1, 5 mm h^{-1} km^{-1} with a simple spatial average. Crosses and circles show profiles with intense DD (IVG<-30) and DI (IVG>30) rates, respectively.

4.3 Horizontal and vertical extent of individual precipitation systems

4.3.1 IVG for individual precipitation systems

Numerous rainfall-rate profiles for inland India were examined to assess how DD profiles are embedded in individual precipitation systems and how the characteristics of those profiles alter the monthly average. Several different rain patterns based on IVG emerged: wide-spread moderately DI stratiform rain, significant DD profiles embedded in deep storms, significant DI profiles in strong convergence zones such as convection at the leading edge of linear mesosale convective systems, moderately DD trailing (or leading) stratiform rain, and relatively small DD convective regions embedded in large stratiform rain area with moderate DI profiles. Figure 23 shows a precipitation system with very heavy rainfall rates (exceeding 100 mm h^{-1}) and high storm heights ($\sim$ 15 km) that contains significant DD and DI profiles simultaneously in the slanting convection. The mean flow obtained from NCEP/NCAR reanalysis data was easterly with weak vertical shear at the closest time and location. The trailing stratiform rain around 79.5°E has DD characteristics. The horizontal extent of the precipitation system should be simultaneously investigated with the vertical extent. The objective of this section is to specify the characteristics of IVG more concretely in light of the climatological features depicted in the previous section. Inland India was chosen for the present analysis mainly to develop the shape characteristics depicted in Chapter 3. Several other factors were also examined: rain type (convective/stratiform), storm height, IVG, near-surface rainfall rate, and the areas of the entire precipitation system, the individual convective elements, and the aggregate convective portion within a system.

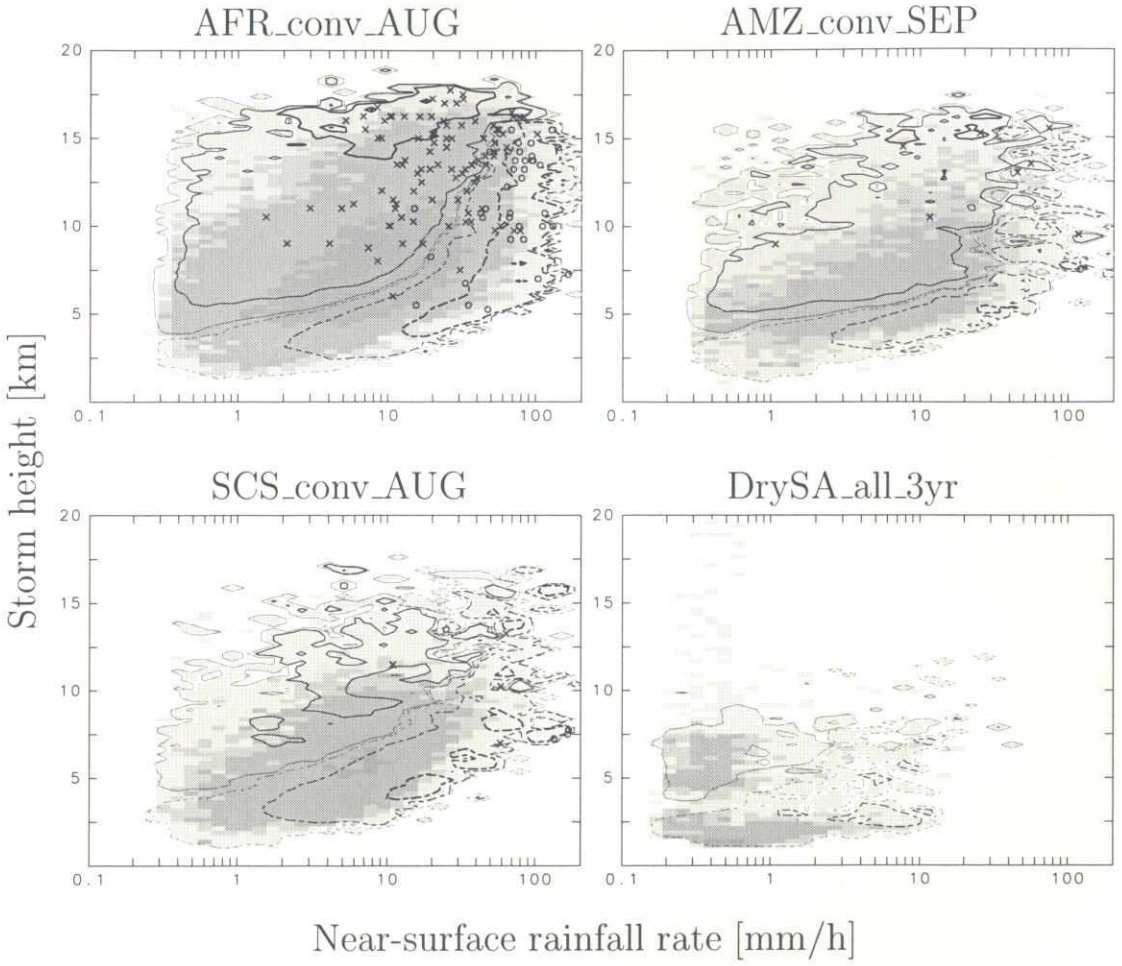

Figure 22. Same as Fig. 21 but for convective rain over northern Africa (AFR_conv_AUG, 10°N–25°N, 20°W–50°E) in August, convective rain over the Amazon River basin (AMZ_conv_SEP, 5°S-EQ, 70°–50°W) in September, convective rain over the South China Sea (SCS_conv_AUG, 10°–20°N, 110°–120°E) in August, and oceanic rain over the eastern part of the South Atlantic (DrySA_all_3yr, off Angola, 20°S–10°S, 0°E–10°E) for all three years.

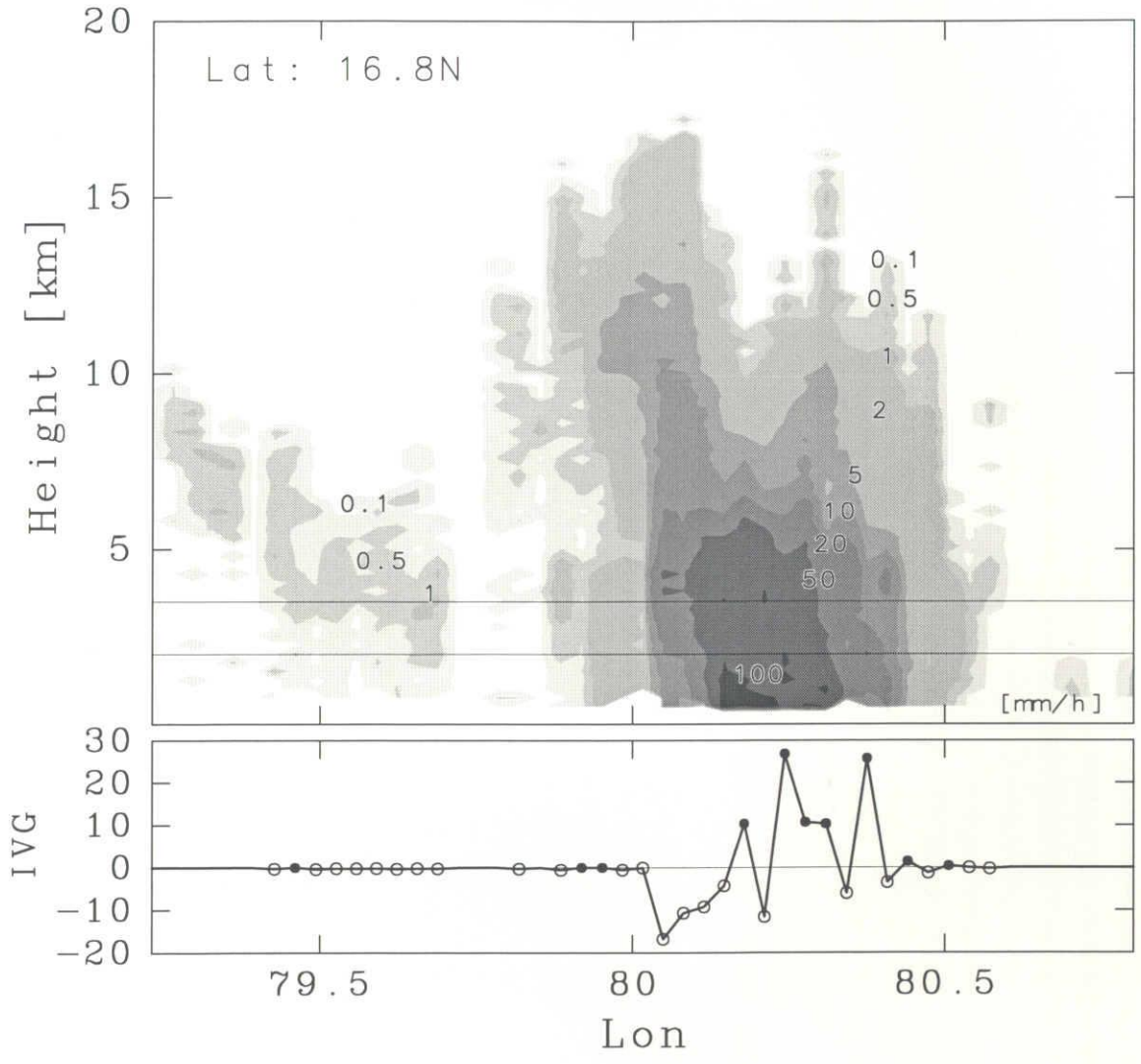

Figure 23. An example of snapshot of a large convective system with significant IVG characteristics. Shading shows rainfall rate over central India at 2:23 LT on 31 Oct. in 1998. The cross-section is along 16.8° N. Two lines indicate altitudes of 2 km and 3.5 km. The lower panel shows the corresponding IVG. Circles and points indicate DD and DI, respectively.

4.3.2 Relationship between rain area and IVG

In this section, the role of the convective area within precipitation systems is investigated. Three years of observations reveal that 99 % of the data with intense gradients (IVG < -10 or > 10 mm h^{-1} km^{-1}) is associated with convective regions. In addition to the significant evaporation in severe convective storms with subsidence warming (Takemi 1999), the effect of strong updrafts is also important (*e.g.,* Dotzek and Fehr 2003). System-dependent characteristics of IVG are examined along with the horizontal area of individual precipitation systems.

Figure 24 shows the convective fraction of systems with significant DD (IVG < -10 mm h^{-1} km^{-1}) and DI (IVG > 10) profiles. The total convective area of a system is the summation of all the individual convective areas embedded in the system. Figure 24 is for May over inland India. It is reasonable to assume that larger precipitation systems had larger convective regions and that those were the main components of the total convective area in those systems. Gray points on large black points in Fig. 24a indicate that most large convective regions are embedded in large systems and include both significant DD and DI profiles. This is more clear in the individual convective area vs. rain area plot shown in Fig. 24b. A large convective region on the scale of an MCS (e.g., larger than 10^4 km^2) often includes both DD and DI profiles, whereas in small convective regions ($\sim$ 100 km^2) significant IVG is absent. Significant DD and DI profiles were also observed in separate convective regions in the same system. A few cases with significant IVG were found in small systems. Many of the significant DD and DI profiles were adjacent in the same large convective region as in Fig. 23. These systems, that have both significant DD and DI profiles, are referred to as "slant cores" for clarity. The proportion of these systems was 1.7 % by number and 22.9 % by area during the three years over India. About one fourth of all rainshafts observed over inland India fall in this category. The systems have a tendency to be DD. Ninety percent of these systems are larger than 10^3 km^2. It was observed that 57 % of large systems (> 10^4 km^2) with significant IVG have slant cores. The interpretation may link the general understanding of oft-studied individual precipitation systems such as

a developing cell containing several convective cells or air mass thunderstorms (*e.g.*, Houze 1993). The lateral transport of water would be important in interpreting the structure, for example, as reported by Rutledge and Houze (1987) that 20 % of the surface precipitation in the stratiform region is due to the influx of hydrometeors from the convective line.

The fractional area of convective rain was on the order of several tens of percent and had a scale dependence (Fig. 24a). There was a limitation as to the extent of the convective regions (thick line, area of convective rain = $2.1(\text{area of rain})^{0.85}$). This boundary was tested for all rain events during the three years and found to be valid (not shown). The area is approximately 70 % in the case of 100 pixels (1.5×10^3 km^2) and 50 % for 1000 pixels (1.5×10^4 km^2). It strongly depends on the thresholds used in a classification method called the "H–method" where a convective core must be significant when compared with the background rain intensity (Awaka *et al.* 1997; Steiner *et al.* 1995). Rain type fraction is closely related to atmospheric heating whose heterogeneity affects dynamic systems (Schumacher and Houze 2003a). A simplified representation for a conglomerate of systems must have information on precipitation systems of various scales (Fabry 1996; Uijlenhoet 2002).

The relationship between rain area and areally averaged IVG was investigated for different climatological regions. Figure 25 shows seasonal variations of the relationship between rain area and IVG over India, northern Africa, the Amazon River basin, and the Brazilian Plateau. Northern Africa (10°–25°N) was chosen as an example of a tropical landmasses with both wet and dry conditions. Generally, over India and Africa in summer, DI profiles decreased as the area increased. This is similar to previous results using rain area density (Fig. 15). Over India, the average IVG line (downward sloping white line in Fig. 25) shifts from DD to DI and back to DD over the period May to October with DI signatures in small, shallow storms and DD signatures in large, deep storms. Many moderate DD and a few significant DD storms characterized May. The IVG of larger systems was close to zero, whereas smaller systems were mostly DI in summer. Laing and Fritsch (1993b) found that the monthly distribution of mesoscale convective complexes (MCCs) over India peaks in the mid-to-late summer. They explained the late summer peak

by the maximum spatial extent of the monsoon. The increase and enlargement of large systems was consistent with the general MCC population. However, these large systems did not show clear DD signature. The rain area was an order of magnitude smaller than that of general MCCs due to the difference between rain, cold cloud shields, and the narrow TRMM PR swath. The major rain mode over northern Africa was DD all through the year. Precipitation systems appeared most frequently in August, which is consistent with the highest occurrence of MCCs around 10°N as reported by Laing and Fritsch (1993a). Over these two continental regions, there was a consistet increase in the large systems but the occurrence of significant IVG was inconsistent reflecting the environmental differences in the generation of quasi-oceanic and continental mesoscale systems there.

The lower two panels show examples over the moist Amazon River basin and the wet and dry Brazilian Plateau. The same downward sloping IVG relationship seen over India and Africa occurs in these dyr, wet, and highly-wet regimes. Over the Amazon River basin, most of the systems are DI except in seasons with relatively less rainfall (i.e., August to November). Small DI systems and large DD systems were seen throughout the year. Over the Brazilian Plateau, large systems were systematically DD in the austral summer. The DD trend was not as clear as the one over Africa.

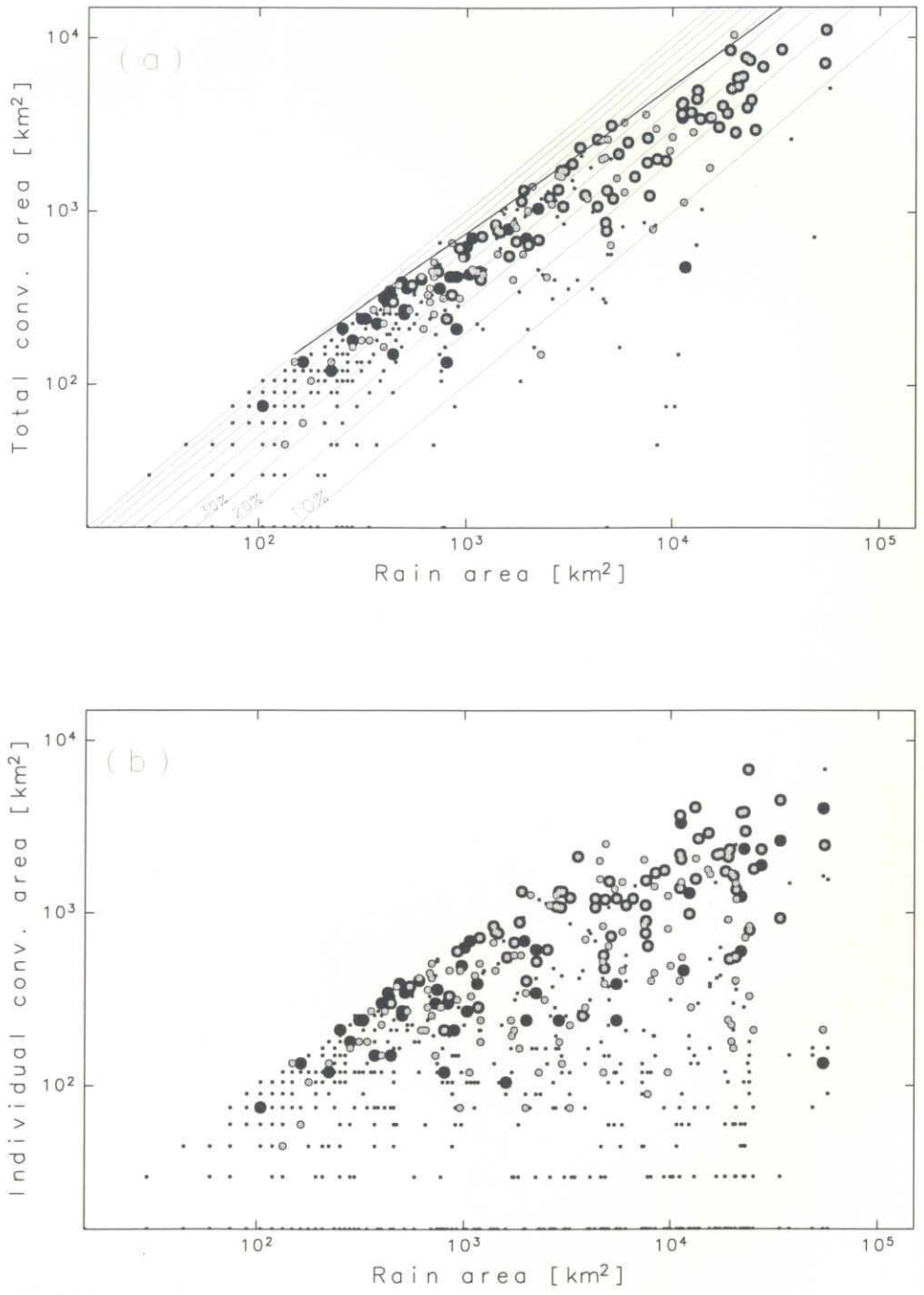

Figure 24. Relationships between rain area and (a) total and (b) individual convective rain areas with significant DD (gray points) and DI profiles (large points) over inland India in May. Small dots represent precipitation systems without significant vertical gradients. Thin lines indicate the convective area fraction.

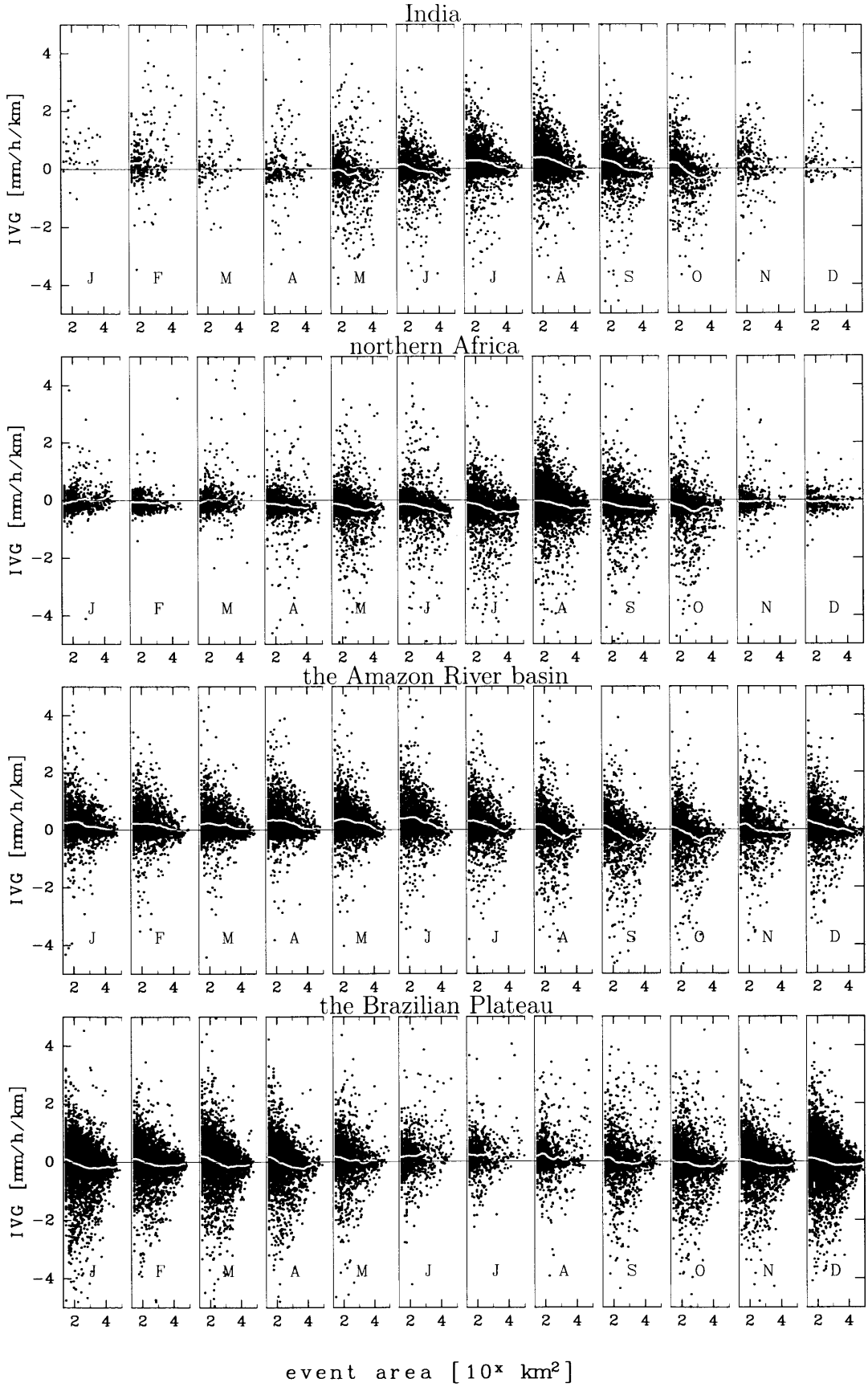

Figure 25. Seasonal variation of the relationship between area and IVG averaged for each system over India, northern Africa, the Amazon River basin, and the Brazilian Plateau. These regions are same as in Fig. 19. The line shows average IVG for 20 log-intervals in rain area from 20 to 10^5 km^2.

4.3.3 Precipitation-system structure during the mature monsoon

Changes in individual systems from the onset to the mature phase of the monsoon over inland India are examined. The number of total, small (< 100 km^2), and large (> 10^4 km^2) systems is shown in Table 2. An area of 100 km^2 represents the "cumulus scale" according to the nomenclature defined by Houze and Cheng (1977) with their minimum detectable signal echo thresholds. The number of profiles of significant IVG (<-10 or >10 mm h^{-1} km^{-1}) is also given in Table 2. The number of all systems and their average area in August was 2.8 times more and 13 % larger, respectiely, than in May. The number of FOVs and rain coverage increased from May to August; however, significant IVG profiles decreased. Though the number of small systems make up about half of the total number of systems (48 % in May and 54 % in Aug), the rain coverage by these cumulus-scale systems is far less (3 % in May and 4 % in Aug). The number of DI profiles in small systems was 5.4 times greater in August than in May. With the rapid increase in the number of moderate DI systems from May to August, the DD fraction decreased from 48 % to 19 %. On the other hand, large systems in August were 1.9 times more in number and 28 % larger in area than in May. In comparison with all systems, rain coverage was about 50 %, whereas, the number of systems decreased from 4 % to 3 % due to the rapid increase of small systems. The DD fraction in large systems changed from 65 % to 54 % from May to August. Furthermore, the number of significant DD (DI) profiles in August was just 53 % (32 %) of that in May in spite of the increase in the number and area of precipitation systems. The standard deviation of IVG was reduced from 3.7 to 1.8 mm h^{-1} km^{-1}. The number of mesoscale and synoptic-scale systems that were moderate DI increased.

The role of significant IVG in a system was investigated. A precipitation system with significant DI profiles (IVG > 10 mm h^{-1} km^{-1}) and no significant DD profiles (IVG < -10) is termed a significant-DI system. This type of system appeared constantly, 7 systems/month on average, throughout the year except in January and December when precipitation events were few. On the other hand, significant-DD systems, those having significant DD profiles (IVG < -10) alone, were observed from May to October ($\sim$ 23 systems/month). In the hot season (phase B in Sec. 4.2), significant-DD systems were few

in comparison with significant-DI systems. The aforementioned slant cores which include both significant DD and DI profiles appeared in summer ($\sim$ 13 systems/month) and in particular during the onset of the monsoon. Figure 26 shows the relationship between IVG in the convective region with that in the stratiform region in May and August. The stratiform part of these systems shows system-dependent variation, even though these systems are classified based on intense gradients that mostly appear in the convective part. The absolute value of IVG in the convective region is larger than that in the stratiform region as expected. In general, they seem to have a linear relationship (sloping upward from left to right). Slant cores are DD especially in the stratiform region in May with the number of slant-core-DD systems reduced by half in August. Most of the IVG in the stratiform portion of significant-DI systems changes from DD to DI. Convective cores aloft in significant-DD systems become moderate, and the DI fraction in the stratiform region increases.

Table 2. The number of systems (No) and embedded DD and DI profiles (FOV_DD, FOV_DI) in May and August. Small and large systems are defined as ones with areas less than 100 km^2 and greater than 10^4 km^2, respectively. The bracket indicates the number of profiles with significant IVG (< -10 or > 10 mm h^{-1} km^{-1}).

	All systems			Small systems			Large systems		
	No	FOV_DD	FOV_DI	No	FOV_DD	FOV_DI	No	FOV_DD	FOV_DI
MAY	1149	19739	11652	559	403	460	47	10326	5524
		(663)	(406)		(7)	(0)		(300)	(246)
AUG	3198	34683	42657	1734	573	2470	90	20904	18057
		(380)	(146)		(10)	(1)		(158)	(79)

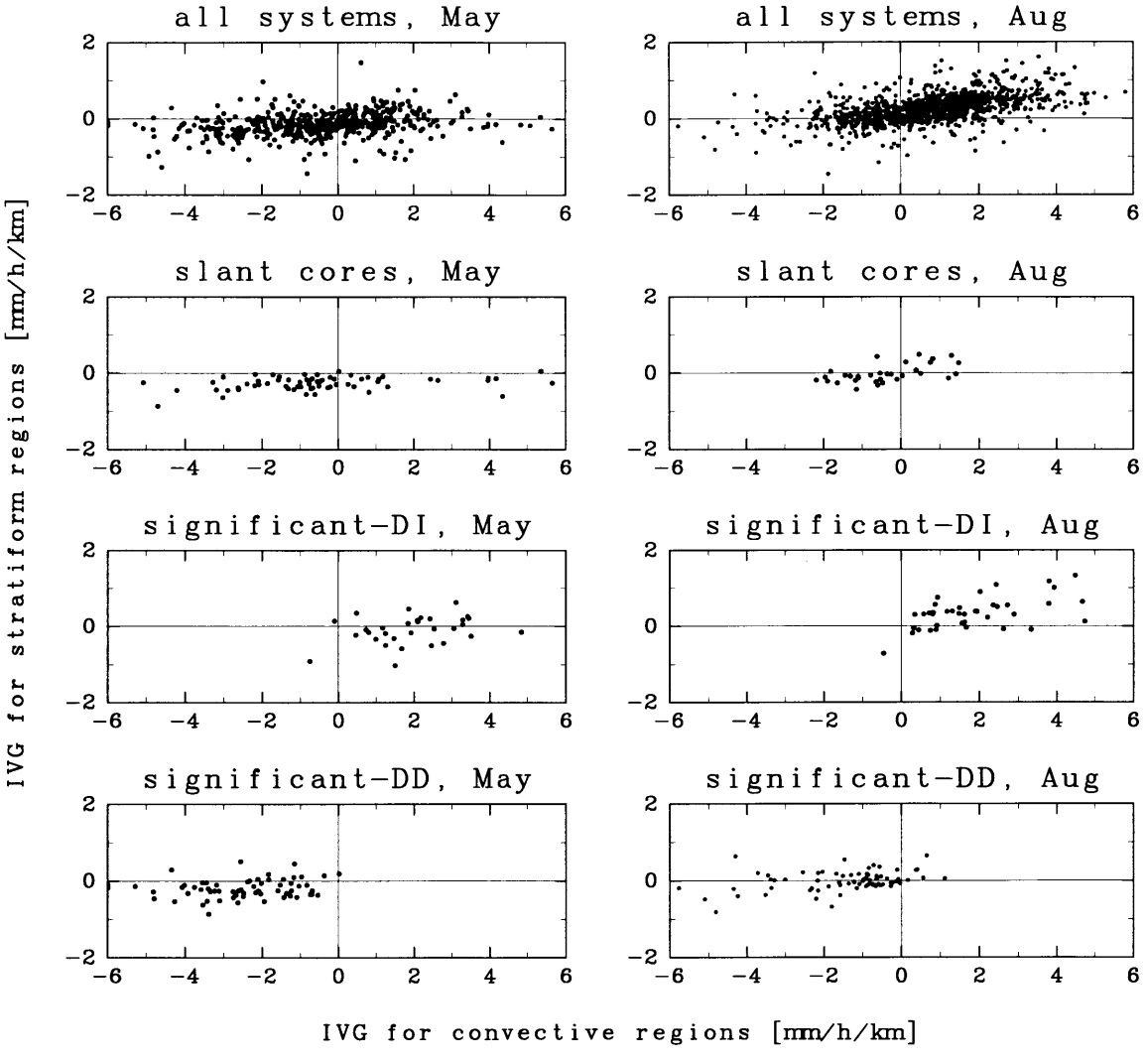

Figure 26. IVG of areally averaged rainfall profiles in each category for convective (abscissa) and stratiform (ordinate) regions. They were obtained for each individual system over India in May and August. Precipitation systems are organized into all systems, slant cores, significant-DI ones, and significant-DD ones, respectively from the top.

5. Summary and discussions

The main objective was to study the spatial and temporal variation of vertical profiles of rainfall rate using observations from the TRMM PR over a large area of Asia and other climatic regions during 1998–2000. We introduce the "index of vertical gradient (IVG)" to describe the vertical gradient of conditional rainfall rate obtained as the difference between the conditional rainfall rate at 2 km and 3.5 km using our 2A25 database (or 4 km using 3A25 output), with due consideration given to sampling numbers, heights of maximum conditional rainfall rate, and brightband effects. Two major categories have been noticed in terms of the vertical gradient in conditional rainfall rate profiles at low levels: downward increasing (DI) and downward decreasing (DD).

The IVG pattern over land is different from that over ocean. Generally, oceanic rain has the DI pattern (IVG>0). IVG over the Maritime Continent is nearly zero. Convective rain over tropical land shows a clear DD pattern (IVG<0) especially in May and June. We focused on rain inland over India and documented notable characteristics. We found that Indian IVG variations are associated with season and the progress of monsoon rainfall. Oceanic rain of DI type pushes the Indian IVG with a DD pattern northward. Analysis using monthly statistical data supported the migration seen every year since the TRMM satellite was launched. The DD migrates northward during onset of the southwest monsoon, responds to rain over the northern part of India including the Thar Desert in the mature period, and withdraws southward during the retrogressing period. IVG correlates strongly with storm height and DD tends to occur when storm height (conditional rainfall rate) is moderately high (strong) during the rainy season. This relation does not apply in the same way for the dry season.

We investigated rainfall and individual IVG over the central parts of India as being representative of tropical inland with relatively low surface roughness. We looked at the consistency between many related parameters such as near-surface rainfall amount,

rain area, storm height, IVG, etc., and their variations. Conditional rainfall rate (storm height) over the Indian inland is strong (high), more than 5 mm h^{-1}, in the month of April and becomes weak (low), less than 3 mm h^{-1}, after the monsoon onset. Rainfall amount decreases in the mature monsoon months, while rain frequency or coverage (rain area density) increases. IVG with low rain area density was more prevalent than those with high rain area density. Isolated rain events with low storm height increased over the Indian subcontinent in August. High storm height does not often appear during June-August not only in the average but also in individual events. Shallow precipitating systems (low storm height and low area density) play a significant role in determining the seasonal variation of IVG patterns over India in summer monsoon.

Furthermore, the seasonal and regional differences of the vertical gradient of rainfall rate were investigated over various climatic regions. Profiles with rainfall-rate peaks aloft often appeared over tropical interior landmasses in summer, corresponding to the seasonal variation of rainfall in the equatorial convective zones. DD profiles broadly appeared as a continental pattern over Africa and the Brazilian Plateau in summer or as a horseshoe-like pattern bordering the height of the wet season over India. The environmental differences between dry, wet, and highly-wet regimes characterized the degree of IVG (i.e., the tendency to be DI, DD, and moderately DI, respectively). Atmospheric moisture was related to precipitation-system structure as reflected in the vertical gradient. In an extremely moist atmosphere during mid to late summer over India, the number of shallow, isolated and weak DI precipitation systems and widespread systems with a moderate IVG increased.

We found several characteristics of vertical profiles of rain such as the seasonal march of IVG patterns. Now, a question may be asked: what does DD imply? Unlike relatively weak DD profiles in stratiform rain, the physical meaning of significant DD profiles is deemed to be due to other possible factors such as strong up and downdrafts and slant cores apart from evaporation. One interpretation of DD may be that the size of rain systems determines IVG. By examining the relationship between IVG and storm height or the spatial extent of rain, we found that DD occurred in well-developed storms. In general,

the IVG for individual systems or profiles decreased (DD tendency) as rain area increased or as storms developed vertically. The above interpretation of vertical gradient may contain the effect of time-averaged duration of raindrops suspended in the air (*e.g.*, Szoke and Zipser 1986). Thus, in large-scale precipitation systems, long-lasting water might be contributing to the time-integrated conditional rainfall-rate profiles and, hence, to IVG. Suspended waterdrops may imply the existence of strong updrafts. These significant DD systems would require strong forcing from the surface to develop deeply. Well-developed systems in May result from the large amount of latent and sensible heat fluxes from the surface and the moist environment in the middle troposphere (*e.g.*, Shinoda and Uyeda 2002). On the other hand, storms with significant DI convective cores alone were also observed in every month over India. Significant-DI systems became a significant minority in the premonsoon season when they made up the greatest portion of severe precipitation systems. These systems may imply the existence of significant low-level convergence. Precipitation systems in the hot season (phase B in Sec. 4.2) were characterized as deep storms with strong rainfall rates and significant DI profiles. In other words, only significant-DI systems with strong low-level convergence might be able to develop under strong atmospheric subsidence in the Hadley cell.

Another possibility involves the spatial distribution of wet and dry regions. The fact that DD appears around the border between dry and wet regions suggests that DD occurs when land is not wet. A major factor producing DD could be evaporation over unsaturated dry regions under cloud bases. In the winter season, IVG (DI pattern) increased corresponding to lower heights of maximum echoes. IVG clearly varied with season, occurring for land and ocean. Monthly IVG shows seasonal variations such as its maximum occurring every August, while storm height is suppressed and almost constant during June-August. The DD variation seems to be related not only to storm height or near-surface conditional rainfall rate but also to the rainfall amount and atmospheric and/or surface wetness.

"Slant cores" were also observed frequently with adjacent profiles that were significantly DD with high storm heights and significantly DI with strong rainfall rates in large

convective areas. Slant cores may be consistent with rearward tilting updraft structures in a mature MCS (*e.g.*, McAnelly *et al.* 1997; Lang *et al.* 2003). Most of them appeared in large systems (90 % were larger than 10^3 km^2) and were noticeably observed in May over India. These systems were specified by the existence of significant IVG and showed system-dependent links in the stratiform and convective patterns. The relationship between these patterns did not show that DD and DI were complementary. They also exhibited a wet to highly wet regime shift from May to August. Abundant moisture makes the regime quasi-oceanic by generating widespread precipitation or cloud shields. The appearance of widespread systems with moderate vertical gradients could be explained by an increase in stratiform rain fraction during the fully developed monsoon due to a more widespread warm, moist boundary layer and more uniform buoyancy (Schumacher and Houze 2003a). Precipitation or cloud systems may be able to change their own regime by reducing the solar insolation under highly wet conditions.

6. Conclusions

By examining seasonal and spatial variations of vertical rain profiles over monsoon Asia, we found that the DD pattern occurs on the border of monsoon rainfall, in the sense that DD progresses northward as the monsoon progresses and withdraws southward as the monsoon recedes. This study suggests that an investigation of mechanisms of the occurrence of DD patterns over the monsoon region may lead to a better understanding of the monsoon variability. This might suggest that IVG is one aspect of monsoon progression.

Then, we further investigated on individual systems or profiles over a variety of scales and climatic regions in order to determine the local or universal characteristics of rain profiles. Generally, IVG was associated with the horizontal/vertical scale of precipitation systems. Deep profiles or large systems were associated with DD signature. The possible factors of DD would be evaporation, the strong updraft, and so on. The PR algorithm assumed that raindrops fall in stagnant air. The different falling velocity causes the maximum rain aloft. On the other hand, shallow or small storms have tendencies to be DI. As notable exceptions, there were deep storms but with DI signature in the premonsoon season and large storms but with moderate DI signature in the mature monsoon period. A series of results showed that the relationship between the scale and the internal structure of precipitation systems have seasonal and spatial variation. The different composition of precipitation systems inferred that the convective activity over dry season is closely associated with atmospheric circulation. Abundant water vapor would change the internal structure even they are similar-scale systems.

The fuller study of rainfall-rate distribution at the lowest levels lies outside the scope of this study due to the uncertainty in the sampling below 2 km. However, investigation of the shallow peaks is also important, for example, to improve the retrieval of rainfall at the surface. Such kind of studies are needed to know the concentration of numerous shallow precipitation systems with echo top around 2 km and to consider the topographic

effect on the sampling over land.

In order to interpret the characteristics of the vertical profiles, understanding the type of precipitation-system and the atmospheric conditions (dry/wet) was important. Further pattern recognition would make the interpretation of the stratiform and convective mixture more meaningful. This suggests that the investigation of average precipitation regimes, statistical analyses or spectral representations would be more informative if precipitation regimes were recognized as being congregations of further parameterized precipitation-system types.

Acknowledgements.

The author would like to express his deepest gratitude to Prof. Kenji Nakamura for his invaluable suggestions and encouragements through the whole period of this study. He wishes to thank Dr. A. Higuchi for discussions and constructive comments, Dr. Kusuma G. Rao and Dr. T. N. Rao for detailed and valuable discussion, Mr. H. Minda for supporting the computer system and Ms. T. Tanaka for her vigorous and generous assistance. Helpful comments from Dr. H. Fujinami are gratefully acknowledged. He also would like to express thank to Dr. Y. Takayabu in Tokyo Univ. for her insight into precipitation structures. Thanks are extended to his colleagues for numerous helpful discussions and sharing undiminished enthusiasms.

The data used in this paper were provided by Japan Aerospace Exploration Agency (previously known as the National Space Development Agency of Japan). The author would like to express their gratitudes to the members of the TRMM project, especially in the Earth Observation Research and application Center.

REFERENCES

Adeyewa, Z. D. and K. Nakamura, 2003: Preliminary study of rainfall and storm structure over africa with TRMM precipitation radar data. *Meteorologische Zeitschrift*, **12**, 197–202.

Atlas, D., R. C. Srivastava and R. S. Sekhon, 1973: Doppler radar characteristics of precipitation at vertical incidence. *Rev. Geophys. Space phys.*, **11**, 1–35.

Awaka, J., 1998: Algorithm 2a23 - rain type classification. *Proc. Symposium on Precipitation Observation from Non-Sum Synchronous Orbit*, Nagoya, Japan, THAS and ESTO, 215–220.

Awaka, J., T. Iguchi, H. Kumagai and K. Okamoto, 1997: Rain type classification algorithm for TRMM precipitation radar. *Proc. IGARSS'97*, Singapore, IEEE, 1633–1635.

Battan, L. J., 1976: Vertical air motions and the Z–R relation. *J. Appl. Meteor.*, **15**, 1120–1121.

Berg, W., C. Kummerow and C. A. Morales, 2002: Differences between east and west pacific rainfall systems. *J. Climate*, **15**, 3659–3672.

Bolen, S. M. and V. Chandrasekar, 2000: Quantitative cross validation of space-based and ground-based radar observations. *J. Appl. Meteor.*, **39**, 2071–2079.

Chang, C. P. and T. N. Krishnamurti, 1987: *Monsoon Meteorology.* Univ. Oxford Press, 544pp.

Dotzek, N. and K. D. Beheng, 2001: The influence of deep convective motions on the variability of Z–R relations. *Atmos. Res*, **59–60**, 15–39.

Dotzek, N. and T. Fehr, 2003: Relationship between precipitation rates at the ground and aloft–a modeling study. *J. Appl. Meteor.*, **42**, 1285–1301.

Fabry, F., 1996: On the determination of scale ranges for precipitation fields. *J. Geophys. Res.*, **101**, 12819–12826.

Fu, Y. and G. Liu, 2001: The variability of tropical precipitation profiles and its impact on microwave brightness temperatures as inferred from TRMM data. *J. Appl. Meteor.*, **40**, 2130–2143.

Fu, Y., Y. Lin, G. Liu and Q. Wang, 2003: Seasonal characteristics of precipitation in 1998 over east asia as derived from TRMM PR. *Adv. in Atmos. Sci.*, **20**, 511–529.

Garstang, M., H. L. Massie, J. Halverson, S. Greco and J. Scala, 1994: Amazon coastal squall lines. Part I: Structure and kinematics.. *Mon. Wea. Rev.*, **122**, 608–622.

Gates, W. L., J. S. Boyle, C. Covey, C. G. Dease, C. M. Doutriaux, R. S. Drach, M. Fiorino, P. J. Gleckler, J. J. Hnilo, S. M. Marlais, T. J. Phillips, G. L. Potter, B. D. Santer, K. R. Sperber, K. E. Taylor and D. N. Williams, 1999: An overview of the results of the Atmospheric Model Intercomparison Project (AMIP I). *Bull. Amer. Meteor. Soc.*, **80**, 29–53.

Gruber, A., X. Su, M. Kanamitsu and J. Schemm, 2000: The comparison of two merged rain gauge-satellite precipitation datasets. *Bull. Amer. Meteor. Soc.*, **81**, 2631–2644.

Heymsfield, G. M., B. Geerts and L. Tian, 2000: TRMM precipitation radar reflectivity profiles as compared with high-resolution airborne and ground-based radar measurements. *J. Appl. Meteor.*, **39**, 2080–2102.

Houze, R. A., 1981: Structures of atmospheric precipitation systems – A global survey. *Radio Science*, **16**, 671–689.

Houze, R. A., 1993: *Cloud Dynamics*. Academic Press, 573pp.

Houze, R. A. and C. P. Cheng, 1977: Radar characteristics of tropical convection ovserved during GATE: Mean properties and trends over the summer season. *Mon. Wea. Rev.*, **105**, 964–980.

Iguchi, T., T. Kozu, R. Meneghini, J. Awaka and K. Okamoto, 2000: Rain–profiling algorithm for the TRMM precipitation radar. *J. Appl. Meteor.*, **39**, 2038–2052.

Kalnay, E., M. Kanamitsu, R. Kistler, W. Collins, D. Deaven, L. Gandin, M. Iredell, S. Saha, G. White, J. Woollen, Y. Zhu, M. Chelliah, W. Ebisuzaki, W. Higgins, J. Janowiak, K. C. Mo, C. Ropelewski, J. Wang, A. Leetmaa, R. Reynolds, R. Jenne and D. Joseph, 1996: The NCEP/NCAR 40-year reanalysis project. *Bull. Amer. Meteor. Soc.*, **77**, 437–471.

Katzfey, J. J. and B. F. Ryan, 1997: Modification of the thermodynamic structure of the lower troposphere by the evaporation of precipitation: A GEWEX cloud system study. *Mon. Wea. Rev.*, **125**, 1431–1446.

Klemp, J. B. and R. B. Wilhelmson, 1978: The simulation of three-dimensional convective storm dynamics. *J. Atmos. Sci.*, **35**, 1070–1096.

Kummerow, C., J. Simpson, O. Thiele, W. Barnes, A. T. C. Chang, E. Stocker, R. F. Adler, A. Hou, R. Kakar, F. Wentz, P. Ashcroft, T. Kozu, Y. Hong, K. Okamoto, T. Iguchi, H. Kuroiwa, E. Im, Z. Haddad, G. Huffman, B. Ferrier, W. S. Olson, E. Zipser, E. A. Smith, T. T. Wilheit, G. North, T. Krishnamurti and K. Nakamura, 2000: The status of the Tropical Rainfall Measuring Mission (TRMM) after two years in orbit. *J. Appl. Meteor.*, **39**, 1965–1982.

Laing, A. G. and J. M. Fritsch, 1993a: Mesoscale convective complexes in Africa. *Mon. Wea. Rev.*, **121**, 2254–2263.

Laing, A. G. and J. M. Fritsch, 1993b: Mesoscale convective complexes over the Indian monsoon region. *J. Climate*, **6**, 911–919.

Lang, S., W. K. Tao, J. Simpson and B. Ferrier, 2003: Modeling of convective-stratiform precipitation processes: Sensitivity to partitioning methods. *J. Appl. Meteor.*, **42**, 505–527.

Lim, Y.-K. and K.-Y. Kim, 2002: Temporal and spatial evolution of the Asian summer monsoon in the seasonal cycle of synoptic fields. *J. Climate*, **15**, 3630–3644.

Liu, G. and Y. Fu, 2001: The characteristics of tropical precipitation profiles as inferred from satellite radar measurements. *J. Meteor. Soc. Japan*, **79**, 131–143.

Manohar, G. K., S. S. Kandalgaonkar and M. I. R. Tinmaker, 1999: Thunderstorm activity over India and the Indian southwest monsoon. *J. Geophys. Res.*, **104**, 4169–4188.

Matejka, T. J., R. A. Houze and P. V. Hobbs, 1980: Microphysics and dynamics of clouds associated with mesoscale rainbands in extratropical cyclones. *Quart. J. R. Met. Soc.*, **106**, 29–56.

McAnelly, R. L., J. E. Nachamkin, W. R. Cotton and M. E. Nicholls, 1997: Upscale evolution of MCSs: Doppler radar analysis and analytical investigation. *Mon. Wea. Rev.*, **125**, 1083–1110.

Nesbitt, S. W., E. J. Zipser and D. J. Cecil, 2000: A census of precipitation features in the tropics using TRMM: Radar, ice scattering, and lightning observations. *J. Climate*, **13**, 4087–4106.

Ninomiya, K. and C. Kobayashi, 1998: Precipitation and moisture balance of the Asian summer monsoon in 1991 partI: Precipitation and major circulation systems. *J. Meteor. Soc. Japan*, **76**, 855–877.

Parker, M. D. and R. H. Johnson, 2000: Organizational modes of midlatitude mesoscale convective systems. *Mon. Wea. Rev.*, **128**, 3413–3436.

Petersen, W. A. and S. A. Rutledge, 2001: Regional variability in tropical convection: Observations from TRMM. *J. Climate*, **14**, 3566–3586.

Rickenbach, T. M., R. Nieto-Ferreira, J. Halverson, D. L. Herdies and M. A. F. S. Dias, 2002: Modulation of convection in the southwestern amazon basin by extratropical stationary fronts. *J. Geophys. Res.*, **107**, doi:10.1029/2000JD000263.

Rosenfeld, D. and Y. Mintz, 1988: Evaporation of rain falling from convective clouds as derived from radar measurements. *J. Appl. Meteor.*, **27**, 209–215.

Rutledge, S. A. and P. V. Hobbs, 1984: The mesoscale and microscale structure and organization of clouds and precipitation in midlatitude cyclones. XII: A diagnostic modeling study of precipitation development in narrow cold-frontal rainbands. *J. Atmos. Sci.*, **41**, 2949–2972.

Rutledge, S. A. and R. A. Houze, 1987: A diagnostic modeling study of the trailing stratiform region of a midlatitude squall line. *J. Atmos. Sci.*, **44**, 2640–2656.

Salles, C. and J.-D. Creutin, 2003: Instrumental uncertainties in Z–R relationships and raindrop fall velocities. *J. Appl. Meteor.*, **42**, 279–290.

Schumacher, C. and R. A. Houze, 2000: Comparison of radar data from the TRMM satellite and Kwajalein oceanic validation site. *J. Appl. Meteor.*, **39**, 2151–2164.

Schumacher, C. and R. A. Houze, 2003a: Stratiform rain in the tropics as seen by the TRMM Precipitation Radar. *J. Appl. Meteor.*, **16**, 1739–1756.

Schumacher, C. and R. A. Houze, 2003b: The TRMM Precipitation Radar's view of shallow, isolated rain. *J. Appl. Meteor.*, **42**, 1519–1524.

Shige, S., Y. N. Takayabu, W. K. Tao and D. E. Johnson, 2003: Spectral retrieval of latent heating profiles from TRMM PR data: Algorithm development with a cloud-resolving model. *J. Appl. Meteor.*, (submitted).

Shinoda, T. and H. Uyeda, 2002: Effective factors in the development of deep convective clouds over the wet region of eastern china during the summer monsoon season. *J. Meteor. Soc. Japan*, 1395–1414.

Short, D. A. and K. Nakamura, 2000: TRMM radar observations of shallow precipitation over the tropical oceans. *J. Climate*, **13**, 4107–4124.

Simpson, J., R. F. Adler and G. R. North, 1988: A proposed Tropical Rainfall Measuring Mission (TRMM) satellite. *Bull. Amer. Meteor. Soc.*, **69**, 278–295.

Sorooshian, S., K.-L. Hsu, X. Gao, H. V. Gupta, B. Imam and D. Braithwaite, 2000: Evaluation of PERSIANN system satellite-based estimates of tropical rainfall. *Bull. Amer. Meteor. Soc.*, **81**, 2035–2046.

Stano, G., T. N. Krishnamurti, T. S. V. V. Kumar and A. Chakraborty, 2002: Hydrometeor structure of a composite monsoon depression using the TRMM radar. *Tellus*, **54**, 370–381.

Steiner, M., R. A. Houze and S. E. Yuter, 1995: Climatological characterization of three-dimensional storm structure from operational radar and rain gauge data. *J. Appl. Meteor.*, **34**, 1978–2007.

Syono, S. and T. Takeda, 1962: On the evaporation of raindrops in a sub-cloud layer. *J. Meteor. Soc. Japan*, **40**, 245–265.

Szoke, E. J. and E. J. Zipser, 1986: A radar study of convective cells in mesoscale systems in GATE. part II: Life cycles of convective cells. *J. Atmos. Sci.*, **43**, 199–218.

Takayabu, Y. N., 2002: Spectral representation of rain profiles and diurnal variations observed with TRMM PR over the equatorial area. *Geophys. Res. Lett.*, **29**, 1–4.

Takemi, T., 1999: Evaporation of rain falling below a cloud base through a deep atmospheric boundary layer over an arid region. *J. Meteor. Soc. Japan*, **77**, 387–397.

Tao, W. K., S. Lang, J. Simpson and R. Adler, 1993: Retrieval algorithms for estimation the vertical profiles of latent heat release: Their applications for TRMM. *J. Meteor. Soc. Japan*, **71**, 685–700.

Trenberth, K. E., 1998: Atmospheric moisture recycling: Role of advection and local evaporation. *J. Climate*, **12**, 1368–1381.

Trenberth, K. E. and C. J. Guillemot, 1998: Evaluation of the atmospheric moisture and hydrological cycle in the NCEP/NCAR reanalyses. *Climate Dynamics*, **14**, 213–231.

Tripoli, G. J. and W. R. Cotton, 1980: A numerical investigation of several factors contributing to the observed variable intensity of deep convection over south Florida. *J. Appl. Meteor.*, **19**, 1037–1063.

Uijlenhoet, R., 2002: *Parameterization of Rainfall Microstructure for Radar Meteorology and Hydrology.* PhD thesis, Wageningen University.

Webster, P. J., 1983: Mechanisms of monsoon low-frequency variability: Surface hydrological effects. *J. Atmos. Sci.*, **40**, 2110–2124.

Webster, P. J., V. O. Magaña, T. N. Palmer, J. Shukla, R. A. Tomas, M. Yanai and T. Yasunari, 1998: Monsoons: Processes, predictability, and the prospects for prediction. *J. Geophys. Res.*, **103**, 14451–14510.

Westcott, N. E. and P. C. Kennedy, 1989: Cell development and merger in an Illinois thunderstorm observed by doppler radar. *J. Atmos. Sci.*, **46**, 117–131.

Williams, E. R., M. E. Weber and R. E. Orville, 1989: The relationship between lightning type and convective state of thunderclouds. *J. Geophys. Res.*, **94**, 13213–13220.

Xie, P. and P. A. Arkin, 1996: Analyses of global monthly precipitation using gauge observations, satellite estimates, and numerical model predictions. *J. Climate*, **9**, 840–858.

Xu, L., X. Gao and S. Sorooshian, 1999: A microwave infrared threshold technique to improve the GOES Precipitation Index. *J. Appl. Meteor.*, **38**, 569–579.

Zipser, E. and K. Lutz, 1994: The vertical profile of radar reflectivity of convective cells: A strong indicator of storm intensity and lighting probability. *Mon. Wea. Rev.*, **122**, 1751–1759.